# DIELECTRIC-PLATE WAVE GUIDE

(MISS) B. V. RAJESWARI*, AND S. K. CHATTERJEE

(*Department of Electrical Communication Engineering, Indian Institute of Science, Bangalore-560012*)

Received on February 31, 1973.

ABSTRACT

*The field in a dielectric wave guide which consists of two lossless dielectric plates placed parallel to each other in free space and excited by an infinite electric line source located exactly mid-way between the two plates is formulated in terms of an infinite integral. The solution of the infinite integral by using the method of contour integration yields the conditions under which the structure behaves as a surface wave guide and or leaky wave guide. Theoretical results are confirmed by experiment.*

## 1. INTRODUCTION

The analysis of fields in a *HSP* guide is usually made by solving the source-free wave equation

$$\nabla^2 \psi + k^2 \psi = 0 \tag{1}$$

in an appropriate coordinate system, where $\psi$ is an eigen function corresponding to the eigen value $k$. In the case of open-type of electromagnetic structures such as surface wave guides, *viz.*, dielectric rod, dielectric-coated metallic plane, Harms-Gouban line, the discrete eigen value solution to the source-free wave equation corresponds to surface waves. It has been shown by Brown [1] that though a surface wave corresponds to a solution of Maxwell's equations and is capable of existing independently of any other field, in practice, it is not possible to launch a pure surface wave uncontaminated by radiation. Hence a surface wave is always accompanied by a radiation field. So, the determination of the complete field on surface wave structure is essentially an excitation problem.

The analysis of source-excited electromagnetic fields for different open boundary structures by several authors [2–16], have contributed significantly to a proper understanding of the phenomena of surface waves, leaky waves, and radiated waves.

Whitmer's [2] analysis of the problem of a dielectric plate of thickness $d$ excited by an infinite thin but infinitely extended current filament, embedded

* Dr. Miss B. V. Rajeswari is at present with the Indian Telephone Industries, Bangalore.

inside the dielectric slab consists of solving the following inhomogeneous wave equation

$$\nabla^2 E_y + k^2 E_y = -\delta(x-b)\,\delta(z) \tag{2}$$

which yields the field $E_y$ outside the dielectric plate in terms of a contour integral as†

$$E_y = \frac{1}{2\pi}\int_{-\infty}^{\infty}\left\{\frac{(p+q)\exp\{q(d+b)\} - (p-q)\exp\{-q(d-b)\}}{(p+q)^2\exp(2qd) - (p-q)^2\exp(-2qd)}\right\}$$

$$\times \exp\{-p(x-d) + ihz\}\,dh \tag{3}$$

where the transverse wave numbers $p$ and $q$ are given in terms of the axial propagation constant $h$ and free space wave number $k_0$ as $p^2 = h^2 - k_0^2$ and $q^2 = h^2 - k^2$ respectively. Whitmer's result does not, however, provide enough information about the field distribution as a whole around the structure.

Cohn *et al*. [3] used the method of steepest descent to evaluate the far field $E_y^R$ asymtotically for any direction outside the slab excited by an infinite line source as in Whitmer's case.

$$E_y^R = \sqrt{\frac{2\pi}{k_0 r}}\,F(\theta)\exp\left(ik_0 r - \frac{i\pi}{4}\right) \tag{4}$$

where.

$$F(\theta) = \frac{1}{2\pi}\,[(p_\theta + q_\theta)\exp\{q_\theta(d+b)\} - (p_\theta - q_\theta)$$

$$\times \exp\{-q_\theta(d-b)\}]/[(p_\theta + q_\theta)^2\exp(2q_\theta d)$$

$$-(p_\theta - q_\theta)^2\exp(-2q_\theta d)]$$

$$p_\theta = -ik_0\cos\theta,\quad q_\theta = [k_0^2\sin^2\theta - k^2]^{\frac{1}{2}}.$$

Tai [4] has analysed the fields produced by a periodic, time-varying current filament located above and parallel to a dielectric-coated conducting plane. The field in the region above the current filament is

$$E_{y1} = \int_{-\infty}^{\infty}\frac{1}{2\pi p}\,[\{q\sinh p(b-d) + p\cosh p(b-d)$$

$$\times \tanh qd\}/(q + p\tanh qd)]\exp\{(-p(x-b))$$

$$+ ihz\}\,dh. \tag{5}$$

---

†*Note*.—The symbols are different from those used by Whitmer but are consistent with those used in the present paper.

Tai's result show that for a thick slab, a surface wave in addition to space wave appears in the vicinity of the dielectric-air interface.

Barone [5] in his analysis of the field due to an electric line source above a dielectric slab has shown that in the evaluation of the contour integral, if the complex poles on the $h$-plane are considered, the residues at these poles correspond to leaky waves. His analysis also leads to the conclusion that though an infinite number of leaky wave resonance exist, it is only a finite number of leaky wave resonances in addition to a finite number of characteristic surface wave modes that may constitute to the field.

The object of the present paper is to report on the analysis of the nature of the fields in dielectric parallel plane wave guide consisting of two parallel dielectric plates placed in air and excited by a line source placed exactly midway between the two plates.

## 2. FORMULATION OF THE PROBLEM

In exciting the parallel plane dielectric wave guide (Fig. 1) by an infinitely extended electric line source, a uniform current of density $\delta(x) F(z) \exp(-i\omega t)\, i\omega\mu_0$ is assumed in the $y$-direction. Since, the source is assumed to be infinitely extended in the $y$-direction and the current is uniform, the only component of the electric field is $E_y$ which satisfies the following wave equations in the six regions (Fig. 1).

$$\nabla^2 E_y + k_0^2 E_y = 0. \tag{6}$$

Outside the sheets in regions I and VI;

$$\nabla^2 E_y + k^2 E_y = 0 \tag{7}$$

inside the dielectric plates in regions II and V;

and

$$\nabla^2 E_y + k_0^2 E_y = -\delta(x)\,\delta(z) \tag{8}$$

in regions III and IV between the two plates; where

$$k_0^2 = \omega^2 \mu_0 \epsilon_0 = (2\pi/\lambda_0)^2 \tag{9 a}$$

$$k^2 = \omega^2 \mu_0 \epsilon_0 \epsilon r = (2\pi/\lambda)^2 \tag{9 b}$$

where $\epsilon_r$ is the dielectric constant of the plates and $\lambda_0 = 3{\cdot}14$ cm.

The solutions of equations (6–8) which take into account all the propagating modes may be expressed in the form of the infinite integral

$$E_y = \int_{-\infty}^{\infty} v(x, h) \exp(+ihz)\, dh \tag{10}$$

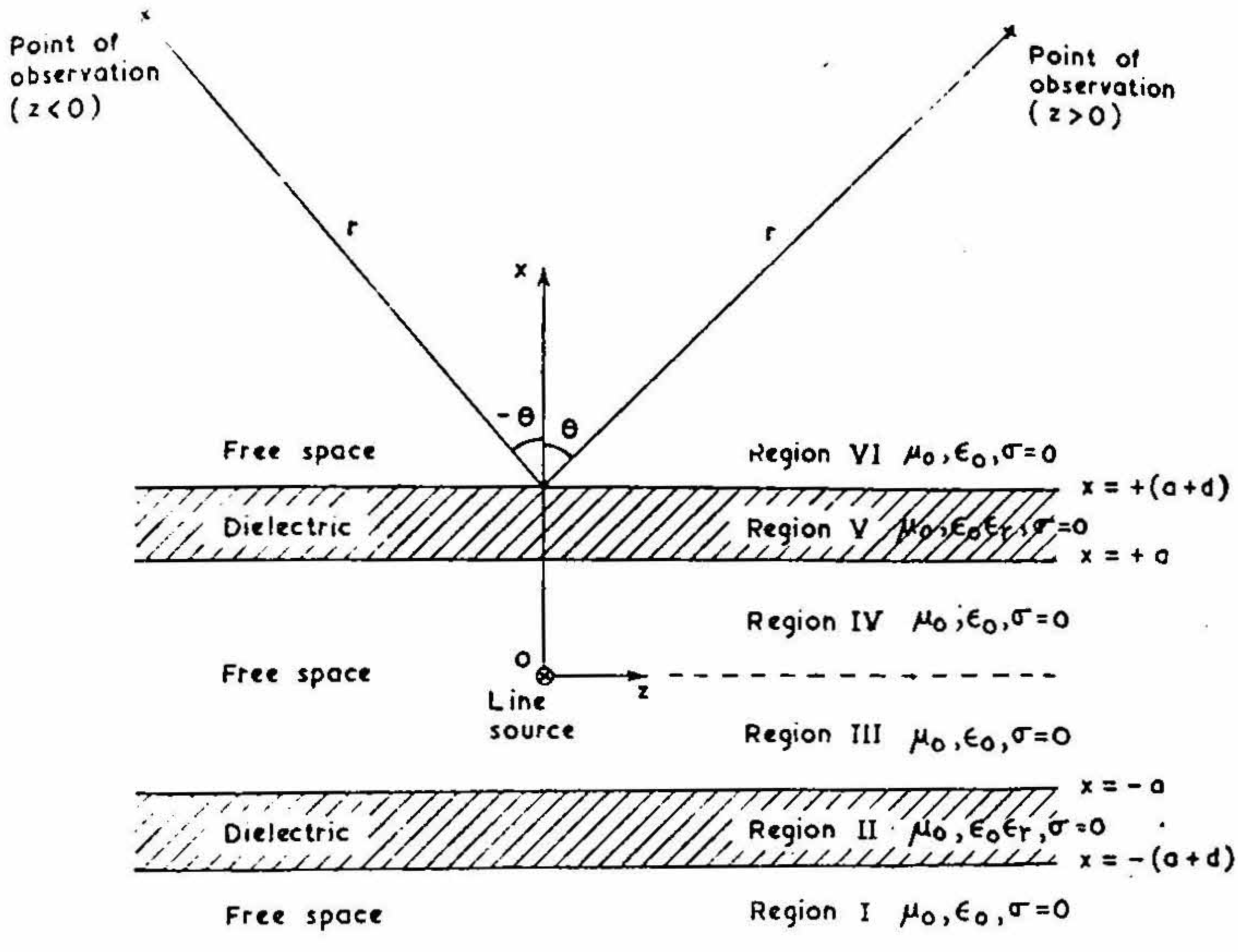


FIG. 1. Coordinate system used in the analysis.

where, $h$ is the axial propagation constant in the $z$-direction and $v(x, h)$ satisfies the following equations:

$$\frac{\partial^2 v(x, h)}{\partial x^2} - (h^2 - k_0^2)\, v(x, h) = 0 \tag{11}$$

in regions I and VI;

$$\frac{\partial^2 v(x, h)}{\partial x^2} - (h^2 - k^2)\, v(x, h) = 0 \tag{12}$$

in regions II and V and

$$\frac{\partial^2 v(x, h)}{\partial x^2} - (h^2 - k_0^2)\, v(x, h) = -\frac{\delta(x)}{2\pi} \tag{13}$$

in regions III and IV,

The components $H_x$ and $H_z$ of the magnetic field $\vec{H}$ derived from $\nabla x \vec{E} = i\omega\mu_0\vec{H}$ are,

$$H_x = -\frac{h}{\omega\mu_0}\int_{-\infty}^{\infty} v(x, h)\exp(+ihz)\,dh \tag{14}$$

$$H_z = \frac{1}{\mu_0\omega}\int_{-\infty}^{\infty}\frac{\partial v(x, h)}{\partial x}\exp(ihz)\,dh. \tag{15}$$

The solutions of equations (11) and (12) are respectively

$$A_1\exp(+px) + B_1\exp(-px) \tag{16 a}$$

and

$$A_2\exp(+qx) + B_2\exp(-qx) \tag{16 b}$$

where

$$p = \pm(h^2 - k_0^2)^{\frac{1}{2}}$$
$$q = \pm(h^2 - k^2)^{\frac{1}{2}}$$

and $A_1$, $A_1$, $B_2$, $B_2$ are arbitrary constants. The solution of the homogeneous counterpart of the inhomogeneous equation (13) is

$$A_3\exp(+px) + B_3\exp(-px)$$
$$= v_1(x, h) + v_2(x, h) \tag{17}$$

The particular integral of the inhomogeneous equation (13) is

$$-v_2\int^{x}\frac{v_1}{W}\cdot\frac{\delta(x)}{2\pi}\,dx + v_1\int^{x}\frac{v_2}{W}\frac{\delta(x)}{2\pi}\,dx \tag{18}$$

where, the Wronskian

$$W = -2A_3B_3p$$

since,

$$\int_{-\infty}^{\infty} f(x)\,\delta(x)\,dx = \int_{-\epsilon}^{+\epsilon} f(x)\,\delta(x)\,dx = f(0)$$

the particular integral reduces to

$$\frac{\exp(+px)}{4p} \quad \text{for} \quad x < 0$$

and

$$\frac{\exp(-px)}{4p} \quad \text{for} \quad x > 0$$

Hence, the most general solution of equation (13) is

$$A_3 \exp(+px) + B_3 \exp(-px). \tag{19}$$

Since there are no reflected waves in regions I and VI and there are reflected waves in all the other regions, $v(x, h)$ for different regions are

$$v(x, h) = \begin{cases} v_1(x, h) = A_1 \exp(+px); & x < -(a+d) \\ v_2(x, h) = A_2 \exp(+qx) + A_3 \exp(-qx) & \\ \qquad -(a+d) < x < -a & \\ v_2(x, h) = A_4 \exp(+px) + A_3 \exp(-px) & \\ \qquad -a < x < 0 & \\ v_4(x, h) = A_6 \exp(+px) + A_7 \exp(-px)\ 0 < x < a & \\ v_5(x, h) = A_8 \exp(+qx) + A_9 \exp(-qx) & \\ \qquad a < x < (a+d) & \\ v_6(x, h) = A_{10} \exp(-px); & (a+d) < x. \end{cases} \tag{20}$$

The ten arbitrary constants are determined by using proper expression for $v(x, h)$ and applying appropriate boundary conditions which are the continuity $E_{tan}$ and $H_{tan}$ at $x = \pm a$ and $x = \pm (a+d)$; continuity of $E_{tan}$ at the source $x = 0$ and the discontinuity of $H_{tan}$ at $x = 0$ by an amount equal to the lunar current density. The discontinuity of $H_2$ or $\partial u/\partial x$ at $x = 0$ is determined from

$$\frac{\partial v(x, h)}{\partial x}\bigg]_{-\epsilon}^{\epsilon} - (h^2 - k_0^2) \int_{-\epsilon}^{\epsilon} v(x, h)\, dx = -\frac{1}{2\pi} \tag{21}$$

which reduce to

$$\frac{\partial v(x, h)}{\partial x}\bigg]_{0-0}^{0+0} = -\frac{1}{2\pi}$$

in the limit $\epsilon \rightarrow 0$.

The constants $A_r = D_r/D$.

(appendix A. 1). Hence, $v(x, h)$ in the different regions are

$$v_1 = q \exp [+ p \{x + (a + d)\}]/\pi x; \qquad x < -(a+d)$$

$$v_2 = [(p + q) \exp [+ q \{x + (a + d)\}] - (p - q) \exp [- q \times \{x + (a + d)\}]]/2\pi x$$
$$-(a + d) < x < -a$$

$$v_3 = [\{(p + q)^2 \exp (+ qd) - (p - q)^2 \exp (- qd)\} \times \exp \{+ p (x + a)\} + (p^2 - q^2) \{\exp (+ qd) - \exp (- qd)\} \times \exp \{- p (x + a)\}]/4\pi p x$$
$$-a < x < 0$$

$$v_4 = [\{(p + q)^2 \exp (+ qd) - (p - q)^2 \exp (- qd)\} \times \exp \{- p (x - a)\} + (p^2 - q^2) \{\exp (+ qd) - \exp (- qd)\} \times \exp \{- p (x - a)\}]/4\pi p x; \qquad 0 < x < a$$

$$v_5 = [(p + q) \exp \{- q [x - (a + d)]\} - (p - q) \exp [+ q \times \{x - (a + d)\}]] 2\pi x$$
$$a < x < (a + d)$$

$$v_6 = q \exp [- p \{x - (a + d)\}]/\pi x$$
$$(a + d) < x$$

where

$$x = \exp (+ pa) \{(p + q)^2 \exp (+ qd) - (p - q)^2 \exp (- qd)\} - \exp (pa) (p^2 - q^2) \exp (+ qd) - \exp (- qd). \tag{22}$$

The main interest is to find the conditions under which the parallel plate-dielectric guide acts as a surface wave guide, a leaky wave guide or as a radiator. Therefore, only the field

$$E_y = \int_{-\infty}^{\infty} \frac{q}{\pi x} \exp [- p \{x - (a + d)\} + ihz] \, dh \tag{23}$$

in the region $x > (a + d)$ outside the guide will be evaluated.

## 3. Roots of the Equation $X = 0$

The integrand in equation (23) possesses singularities, *viz.*, (i) the poles occurring at $x(h) = 0$ and (ii) the branch points at $h = \pm k_0$ where $h = \beta + i\alpha$. The roots of the equation (22), $x = 0$, *i.e.*,

$$q \coth qd = \frac{b^2 \exp(-2pa) - (2p^2 - b^2)}{2p} \tag{24}$$

$$b^2 = k^2 - k_0^2$$

may be such that the propagation constant $h$ may be real, imaginary or complex.

3.1. *The real roots of $X = 0$.*—Several cases may arise depending on the range of $h$. All the real roots in the range $-\infty < h < +\infty$ cannot be found by using one equation since $p$ and $q$ range over real and imaginary values as $h$ varies from $-\infty$ to $+\infty$. Since all the roots of equation (24) occurs in pairs it is sufficient to determine the roots in the range $0 < h < +\infty$.

*Case* (i) $0 < h < k_0$,

$$p = \pm iw$$
$$q = \pm i(b^2 + w^2)^{\frac{1}{2}}$$
$$w = (k_0^2 - h^2)^{\frac{1}{2}}. \tag{25}$$

Therefore equation (24) reduces to

$$(b^2 - w^2)^{\frac{1}{2}} \cot (b^2 + w^2)^{\frac{1}{2}} \cdot d = -\frac{b^2 \sin 2wa}{2w} \tag{26 a}$$

and

$$\{\mp b^2 \cos 2wa \mp (2w^2 + b^2)\}/2w = 0 \tag{26 b}$$

where, the second equation (26 *b*) can be reduced to

$$b^2 (1 + \cos 2wa) = -2w^2$$

which cannot have real roots. Hence there can be no real root of $X = 0$ in the range $0 < h < k_0$.

*Case* (ii) $k_0 < h < k$ *i.e.*, $0 < w < b$

The equation (24) takes the form

$$(b^2 - w^2)^{\frac{1}{2}} \cot (b^2 - w^2)^{\frac{1}{2}} \cdot d - \{b^2 \exp(-2wa) - (2w^2 - b^2)\}/2w$$
$$= f_1(w) = 0 \tag{27}$$

where

$$p = +(h^2 - k_0^2)^{\frac{1}{2}} = w$$

$$q = \pm i\,(b^2 - w^2)^{\frac{1}{2}}$$

and

$$(b^2 - w^2)^{\frac{1}{2}} \cot (b^2 - w^2)^{\frac{1}{2}} . d - \{- b^2 \exp (2wa) + (2w^2 - b^2)\}/2w$$
$$= f_2(w) = 0 \tag{28}$$

where

$$p = -w \quad \text{and} \quad q = \pm i\,(b^2 - w^2)^{\frac{1}{2}}.$$

*Case* (iii) $k < h < \infty$

The equation (24) assumes the form

$$(w^2 - b^2)^{\frac{1}{2}} \coth (w^2 - b^2)^{\frac{1}{2}} . d - [b^2 \exp (\mp 2wa) - (2w^2 - b^2)]/$$
$$\mp 2w = 0 \tag{29}$$

where

$$p = \pm w$$

and

$$q = \pm (w^2 - b^2)^{\frac{1}{2}}.$$

In this region there is no solution (equation 29).

In order to determine if the end points of the range $(0, k_0)$, $(k_0, k)$, $(k, \infty)$, $(0, -k_0)$, $(-k_0, -k)$ and $(-k, -\infty)$, *i.e.*, $0, \pm k_0, \pm k$ are roots the corresponding values are substituted in equation (24) to find whether the equation is satisfied. The cases when $0, \pm k_0$, or $\pm k$ is a root are discussed below.

*Case* (iv) $h = 0$

$p = \pm ik_0$, $q = \pm ib$. The equation (24) fields

$$k \cot kd = \frac{-b^2 \sin 2k_0 a}{2k_0}$$

and as

$$2k_0 a = \frac{k^2 + k_0^2}{b^2} = \frac{k^2 + k_0^2}{k^2 - k_0^2}$$

which is not satisfied. Hence, $h = 0$ is not a root.

*Case* (v) $h = k_0$

$$p = 0, \quad q = \pm ib.$$

Hence, $h$ equation (24) shows that $h = k_0$ is a root when $b \cot bd = \infty$ or $bd = n\pi$, $n = 1, 2, 3 \ldots$

*Case* (vi)

$$h = +k$$

$$p = \pm b, \quad q = 0.$$

As $q \to 0$, the L.H.S. of equation (24) becomes

$$\underset{q \to 0}{\mathrm{Lt}}\; q \coth qd = \underset{q \to 0}{\mathrm{Lt}} = \frac{q}{\tan qd} = \frac{1}{d}$$

and the R.H.S. of equation (24) tends to

$$\pm b \{\exp(\pm 2ba) - 1\}/2.$$

Hence a root occurs at $h = +k$, when

$$\pm \frac{1}{d} = \pm b \{\exp(\pm 2ba) - 1\}/2.$$

The upper sign holds good when

$$p = +(h^2 - k_0^2)^{\frac{1}{2}}$$

and the lower sign holds when

$$p = -(h^2 - k_0^2)^{\frac{1}{2}}.$$

Numerical evaluation shows that real roots for $f_1(w) = 0$ exist for discrete values of $w$ with $k_0 = 200$ radians/m, $k = 320$, 400 radians m; '$a$' varying from 0·02 to 0·1 m and '$d$' ranging from 0·0016 m to 0·0127 m. Whereas real roots exist for $f_2(w) = 0$, only for $k = 320$ radians/m, $d = 0{\cdot}0127$ m and '$a$' ranging from 0·02 m to 0·06 m with $k_0 = 200$ radians/m.

3.2. *The imaginary roots of* $X = 0$.—By substituting $p = \pm iw$ and $q = \pm i(w^2 - b^2)^{\frac{1}{2}}$ in equation (24) it reduces to

$$b^2 \sin 2wa = 0,$$

and

$$-4w^2 x \cot xd = b^2 \cos 2wa + 2w^2 + b^2$$

which indicate that no imaginary root of equation (24) exists giving real $w$.

3.3. *The complex roots.*—Substituting $p = x^* + iy^*$, $q = u + iv$ in equation (24) and separating the real and imaginary parts, it is found that complex roots occur when

$$\frac{2\,(uf + vg)}{1 + \tanh^2 ud \cot^2 vd} - \frac{x^* S - x^* T}{x^{*2} + y^{*2}} = F_1(x^*, y^*) = 0 \tag{30}$$

and

$$\frac{2\,(vf - ug)}{1 + \tanh^2 nd \cot^2 vd} - \frac{(y^* S + x^* T)}{x^{*2} - y^{*2}} = F_2(x^*, y^*) = 0 \tag{31}$$

where

$$\begin{aligned}
f &= \tanh ud \operatorname{cosec}^2 vd \\
g &= \cot ud \operatorname{sech}^2 vd \\
S &= b^2 \exp(-2x^* a) \cos 2y^* a - 2\,(x^{*2} - y^{*2}) + b^2 \\
T &= b^2 \exp(-2x^* a) \sin 2y^* a + 4x^* y^* \\
u &= \frac{1}{\sqrt{2}} \left[\{(x^{*2} - y^{*2} - b^2)^2 + 4x^{*2} y^{*2}\}^{\frac{1}{2}} + (x^{*2} - y^{*2} - b^2)\right]^{\frac{1}{2}} \\
v &= \frac{1}{\sqrt{2}} \left[\{(x^{*2} - y^{*2} - b^2)^2 + 4x^{*2} y^{*2}\}^{\frac{1}{2}} - (x^{*2} - y^{*2} - b^2)\right]^{\frac{1}{2}}.
\end{aligned} \tag{32}$$

3.4. *Solution of equations giving pure real roots.*—For $h$ varying from $k$ to $+\infty$, *i.e.*, $w$ varying from $b$ to $+\infty$, equation (29) has no solution. The approximate values of the roots of equations (27) and (28) are found graphically (Figs. 2 and 3). In order to get the accurate values of the roots from the approximate values, successive bisection method (Appendix A-2) has been used.

3.5. *Solution of equations giving complex roots of $X = 0$.*—$F_1(x^*, y^*)$, and $F_2(x^*, y^*)$ are plotted (Figs. 4 and 5) versus $y^*$ for discrete values of $x^*$ $(x_1, x_2 \ldots x_n)$. The pairs of $(x_n, y_n)$ which satisfy $F_1(x^*, y^*) = 0$ or $F_2(x^*, y^*) = 0$ are determined from Figs. (4) and (5). These values of $y_n$ are plotted *versus* $x_n$ (Fig. 6) in which $F_1(x^*, y^*) = 0$ and $F_2(x^*, y^*) = 0$ are shown as functions $Y_1 = P_1(x^*)$ and $Y_2 = P_2(x^*)$. The points of intersection of $Y_1$ and $Y_2$ have their $x$ and $y$ satisfying both $F_1 = 0$ and $F_2 = 0$. These values of $x^*$ and $y^*$ gave the approximate roots of (30) and (31). In order to improve the accuracy of the roots, $F_1(x^*, y^*)$ and $F_2(x^*, y^*)$

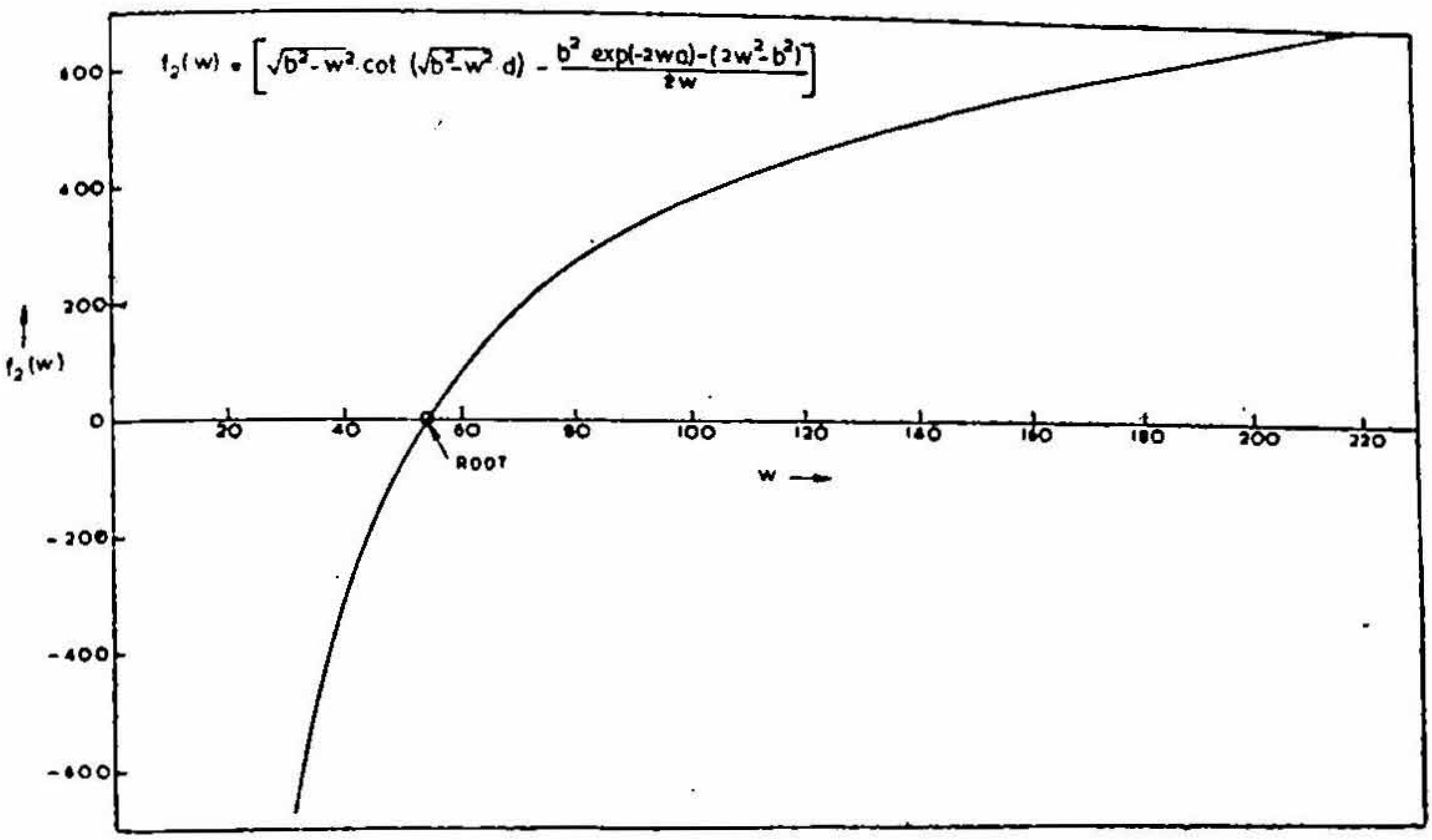


FIG. 2. Plot of $f_2(w)$. $a = 0 \cdot 02$ m, $d = 0 \cdot 0016$ m, $k_0 = 200$ radians per metre, $k = 320$ radians per metre.

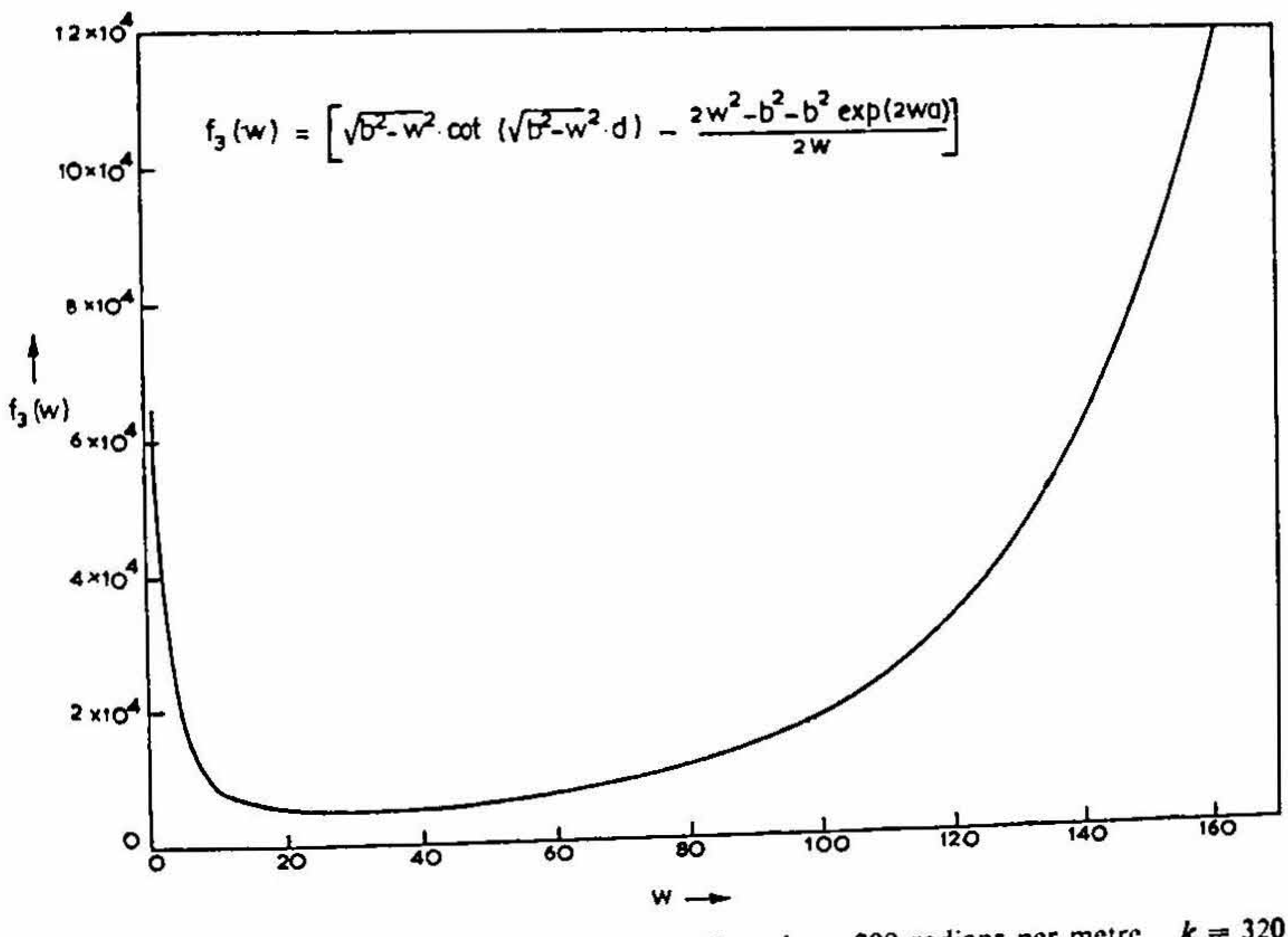


FIG. 3. Plot of $f_3(w)$. $a = 0 \cdot 02$ m, $d = 0 \cdot 0016$ m, $k_0 = 200$ radians per metre, $k = 320$ radians per metre

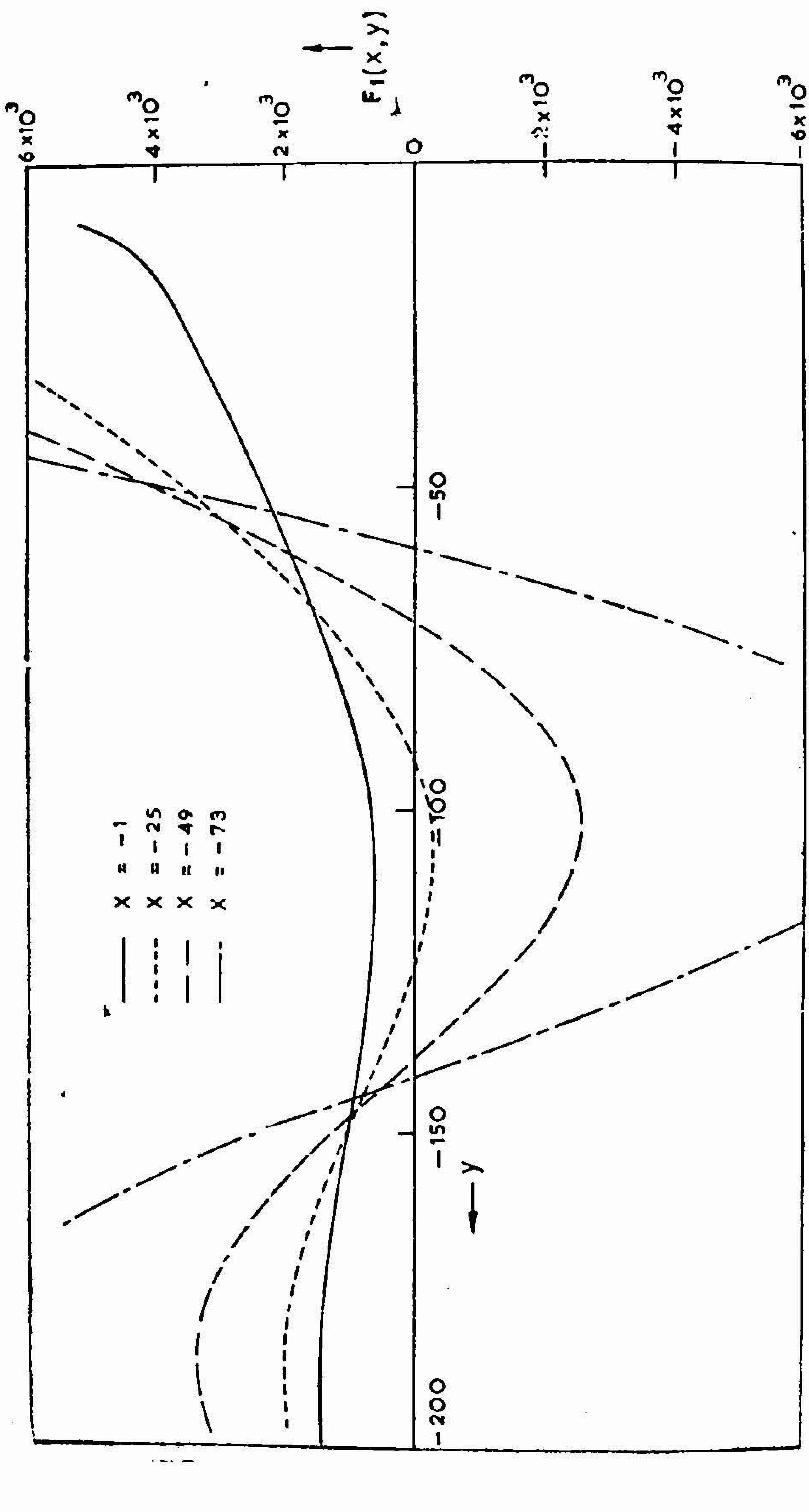


FIG. 4. Plot of $F_1(x, y)$ as a function of $y$ for different values of $x$. $a = 0 \cdot 02$ m, $d = 0 \cdot 0016$ m, $k_0 = 200$ radians per metre, $k = 320$ radians per metre.

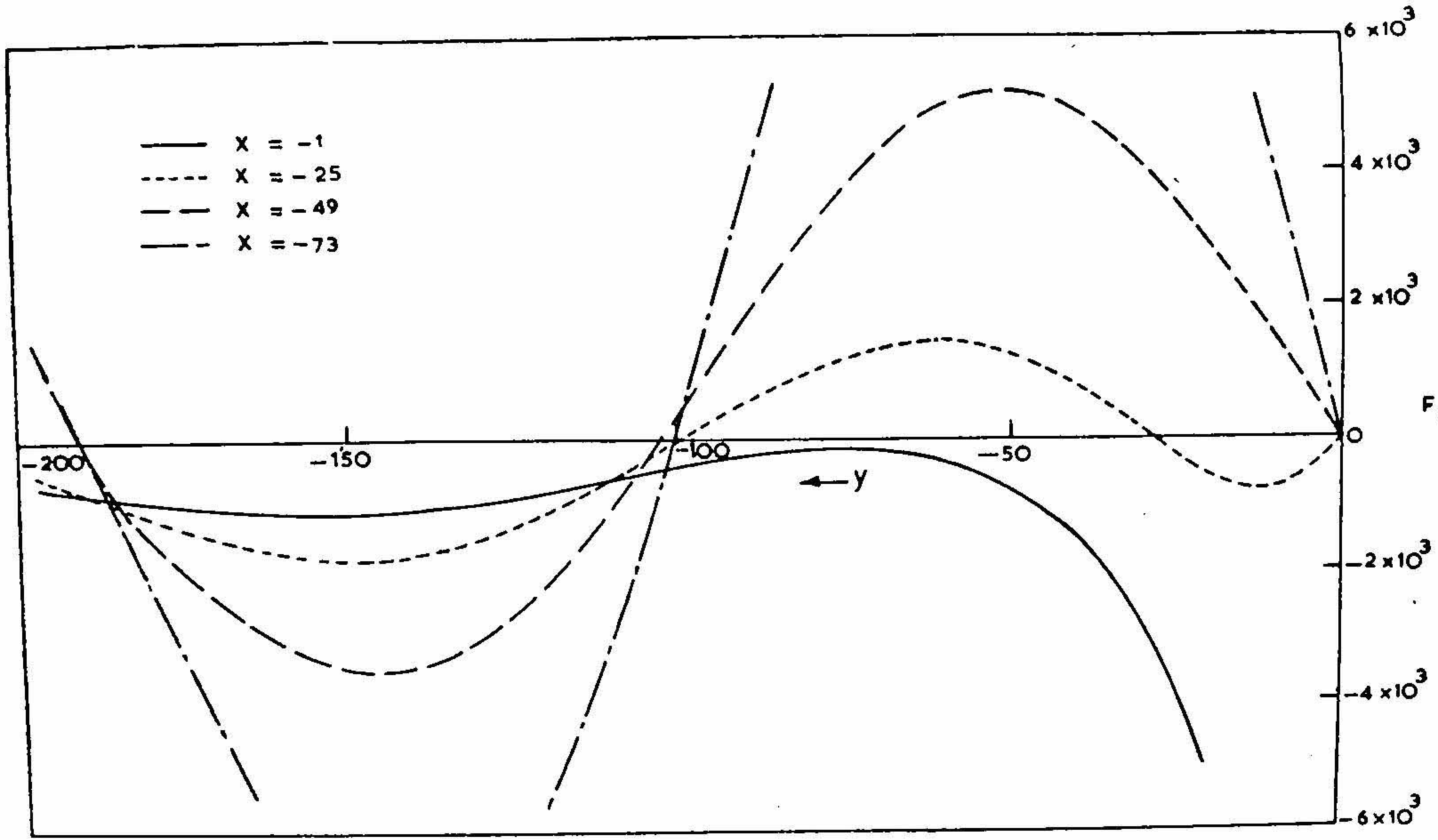


FIG. 5. Plot of $F_2$ $(x, y)$ as afunction of $y$ for fixed values of $x$. $a = 0\cdot02$ m, $d = 0\cdot0016$ m. $k_0 = 200$ radians per metre, $k = 320$ radians per metre.

are evaluated at closer and closer values of $x^*$ and $y^*$ in the neighbourhood of the roots. From these evaluations, points on the curves (Figs. 4 and 5) are found near the roots when these points are close enough, the curves of $F_1(x^*, y^*) = 0$ and $F_2(x^*, y^*) = 0$ can be approximated to straight lines. The coordinates of the point of intersection yield $x^*$ and $y^*$ values of the roots. The complex roots have been determined for $a = 0{\cdot}02$ m, $0{\cdot}03$ m, $d = 0{\cdot}0064$ m, $k_0 = 200$ radians/m and $k = 320$ radians/m (Table I).

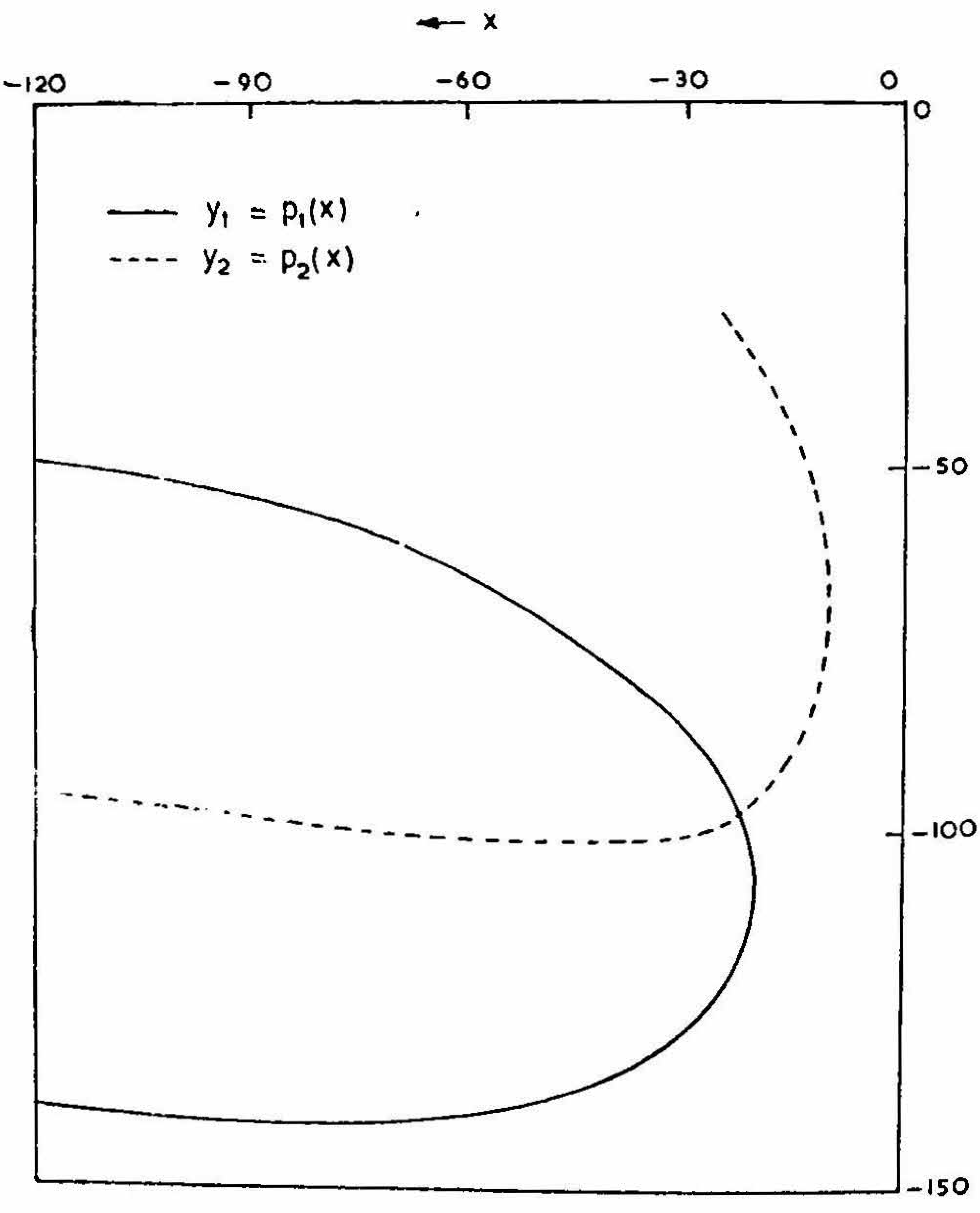


FIG 6

TABLE I

*Values of* x* *and* y* *for complex roots of* $X = 0$

$d = 0{\cdot}0064$ m, $k_0 = 200$ radians/m, $k = 320$ radians/m.

| $a = 0{\cdot}02$ m | | $a = 0{\cdot}03$ m | |
|---|---|---|---|
| $x^*$ | $y^*$ | $x^*$ | $y^*$ |
| − 4·1865 | − 76·726 | − 1·363 | − 51·888 |
| − 23·7475 | − 218·068 | − 9·207 | − 151·959 |
| − 50·358 | − 345·234 | − 20·243 | − 247·928 |
| − 64·445 | − 450·758 | − 34·994 | − 329·2729 |

## 4. DISCUSSION OF THE ROOTS OF $X = 0$

The nature of the fields is determined by the values of $h$ and $p$ corresponding to the roots. The different cases are:

*Case* (i) *Surface waves.*—The roots of equation (27) yield positive real values of $p$. The waves corresponding to these roots alternate exponentially in the $x$ direction and travel without attenuation in the $z$-direction with phase velocity less than the free space velocity as $h > k_0$. These waves are the surface waves. For $0 < w < b$, $d = 0{\cdot}0064$ m there is only one surface wave mode (Fig. 7). The plot of '$p$' *vs* '$a$' (Fig. 8) shows that the surface wave become more and more tightly bound as $p$ becomes larger with '$a$' decreasing.

The evaluation of the residues at the surface wave pole $h = h_0$ given by

$$q_0 \exp\left[- p_0 \{x - (a + d)\} + ih_0 z\right] / \pi \left.\frac{dx}{dh}\right|_{h=h_0}$$

show that the modulus of $2\pi i X$ residue at $x = a + d$ decreases with increase of spacing '$a$' between the plates. This indicates that with the increase of '$a$', the surface waves become more and more loosely bound and also the power in the surface wave decreases. The residues at the poles derived from the surface wave roots are given in Table II for some values of '$d$' and '$a$'.

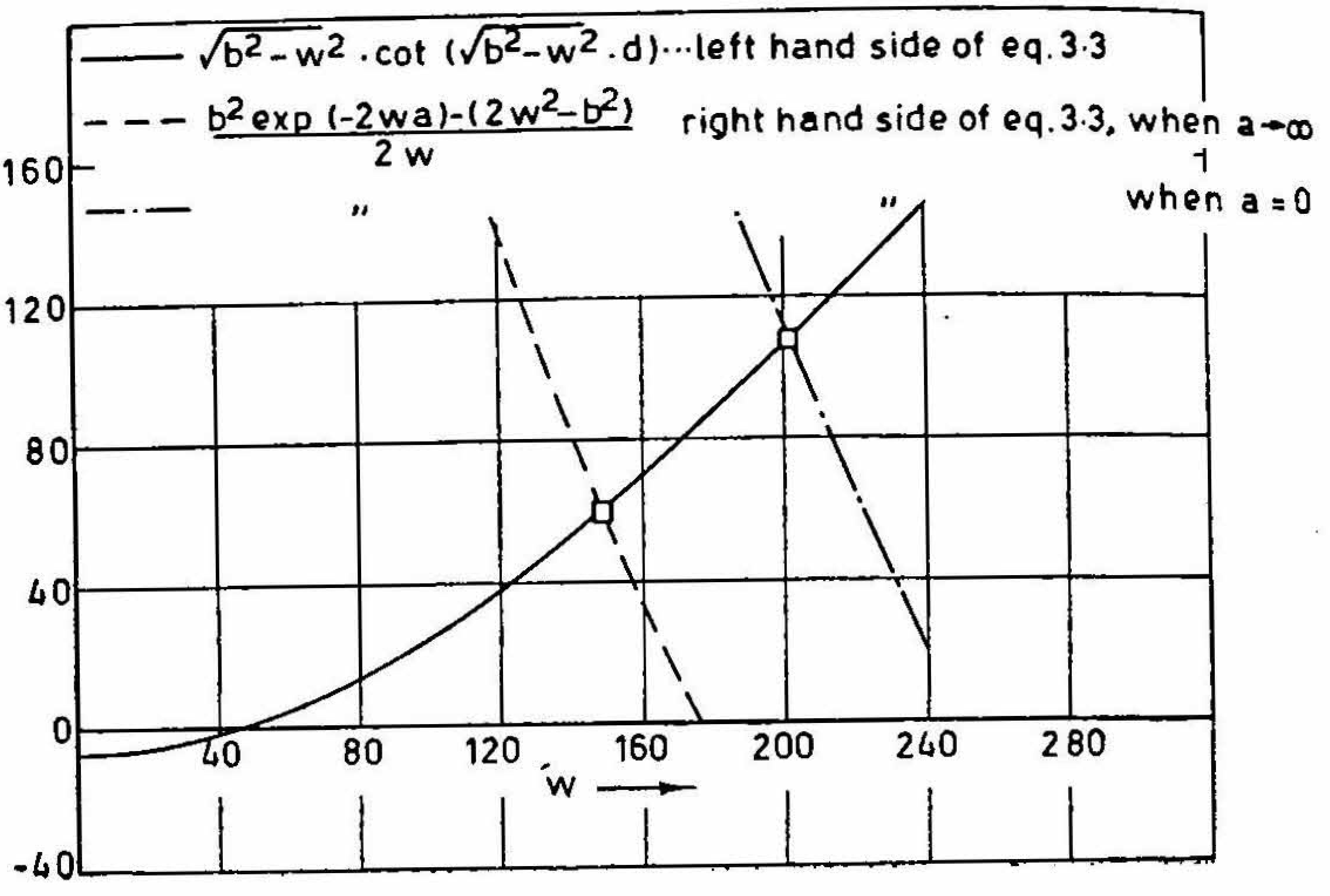


FIG. 7. Roots of $f_1(w) = 0$, $d = 0{\cdot}0064$ m, $k_0 = 200$ radians per metre, $k = 320$ radians per metre.

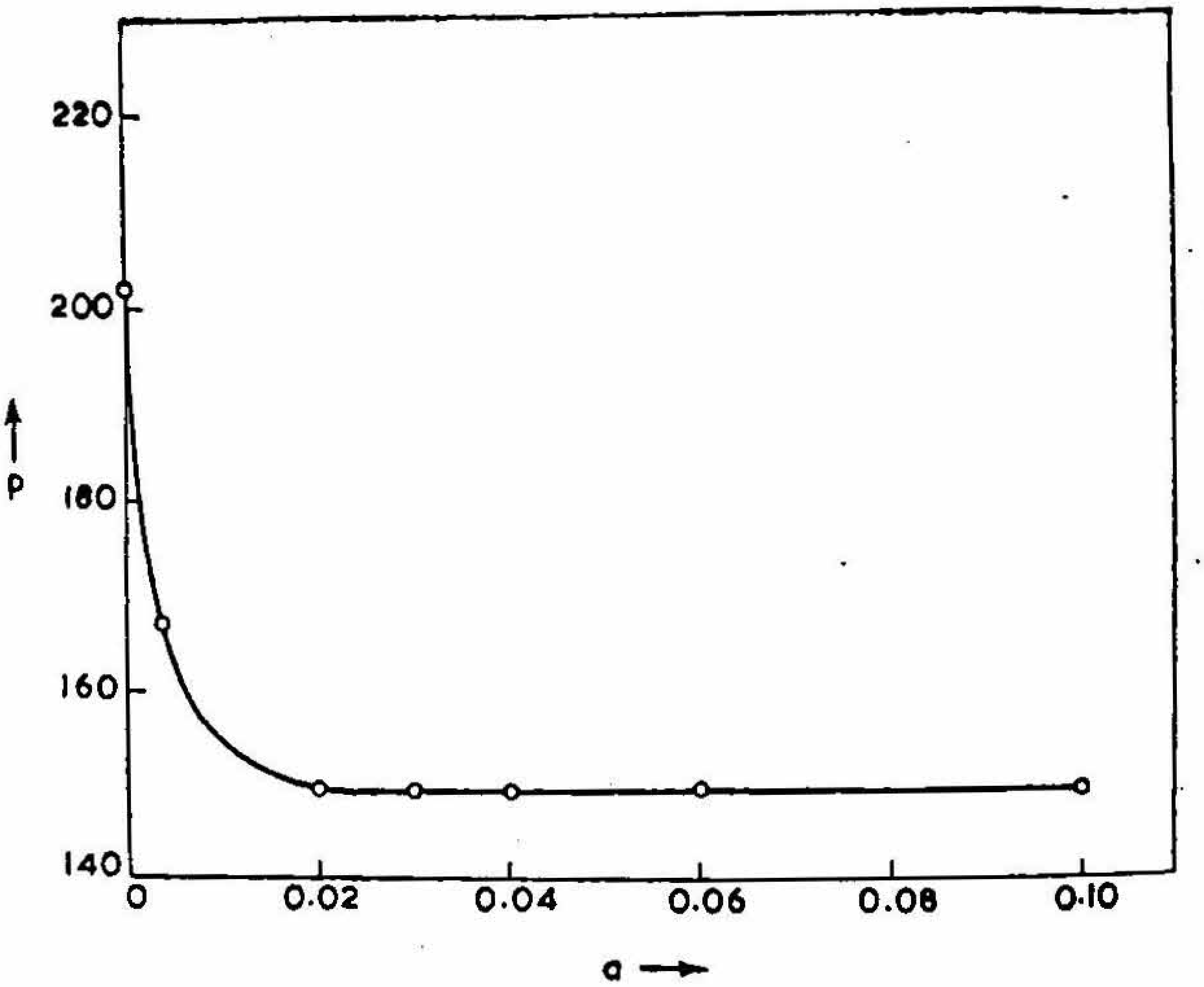


FIG. 8. Plot of $p$ versus $a$. $d = 0{\cdot}0064$ m, $k_0 = 200$ radians per metre, $k = 320$ radians per metre.

TABLE II

*Values of modulus of* $2\pi i$ *X Res. at the surface wave poles*

$k_0 = 200$ radians/m, $k = 320$ radians/m, $x = a + d$

| $d\,(m)$ | $a\,(m)$ | Modulus of $2\pi i$ X Res. |
|---|---|---|
| 0·0016 | 0·02 | $0{\cdot}33 \times 10^{-1}$ |
| | 0·04 | $1{\cdot}43 \times 10^{-2}$ |
| | 0·10 | $0{\cdot}84 \times 10^{-3}$ |
| 0·0032 | 0·02 | $0{\cdot}24 \times 10^{-1}$ |
| | 0·04 | $0{\cdot}21 \times 10^{-2}$ |
| | 0·10 | $1{\cdot}77 \times 10^{-5}$ |
| 0·0064 | 0·02 | $0{\cdot}64 \times 10^{-2}$ |
| | 0·04 | $0{\cdot}33 \times 10^{-3}$ |
| | 0·10 | $0{\cdot}42 \times 10^{-7}$ |
| 0·0095 | 0·02 | $0{\cdot}22 \times 10^{-2}$ |
| | 0·04 | $0{\cdot}6 \times 10^{-4}$ |
| | 0·10 | $1{\cdot}09 \times 10^{-9}$ |

*Case (ii) Growing waves.*—The roots of equation (28) give positive real values of $h$ and negative real values of $p$. These roots give rise to waves growing exponentially in the $x$-direction and travelling unattenuated in the $z$-direction with a phase velocity less than that of plane waves in free space. These waves are physically inadmissible and do not figure in the evaluation of the field as they are associated with the poles lying in the lower leaf of the two-leaved Riemanian plane.

*Case* (iii) *Leaky waves.*—The complex roots evaluated with the help of $F_1(x^*, y^*) = 0$, $F_2 = (x^*, y^*) = 0$ show that (Table I) both the real and imaginary parts of $p$ are negative. The real and imaginary parts of $h$ being positive, the waves associated with these complex poles travel in the $x$-direction growing exponentially but attenuating exponentially in the $z$-direction. These are the leaky wave modes which exist within wedge (Section which is formed on one side by the outer surface of the guide) and the other plane making an angle with the surface.

## 5. EVALUATION OF THE FIELD

The total field consists of the sum of the residues at the poles and the field associated with the branch-cut integration. The residue at any pole $h_0$ represent physically realisable waves when $Re\,p > 0$ and $Im\,h > 0$. In evaluating the infinite integral (equation 23), the double-valued nature of the integrand is removed by assuming a two-leaved Riemanian surface for $h$, the top leaf corresponding to $Re\,(-p) < 0$, and the bottom leaf being designated by $Re\,(-p) > 0$, the branch-cut is designated by $Re\;(-p) = 0$ which reduces to $\alpha\beta = k_0' k_0''$ with $\beta < k_0'$ if $k_0 = k_0' + ik_0''$, and $h = \beta + i\alpha$.

The top leaf of the $h$-plane with the contour $C_0$ which includes poles associated with physically realisable waves, the branch-cut and the branch points are shown in Fig. 9. The complex poles that give rise to outward propagating physically realisable wave can occur in the cross-hatched region in the first quadrant ($z > 0$). But as $k_0'' \to 0$, the area of the cross-hatched region $\to 0$. So, no complex poles can exist on the top leaf. The integral along the dotted infinite semi circle being zero, the integral (equation 23) becomes equal to $2\pi i X$ Res. at the poles included by the contour $C_0$ and the contribution by the branch-cut. The integral is evaluated by the saddle-point method [17].

7.1. *The saddle-point method.*—By making the transformation

$$h = k_0 \sin \tau$$

with

$$p = -ik_0 \cos \tau$$

$$\tau = \xi + i\eta$$

and changing to polar coordinates

$$x - (a + d) = r \cos \theta$$

$$z = r \sin \theta$$

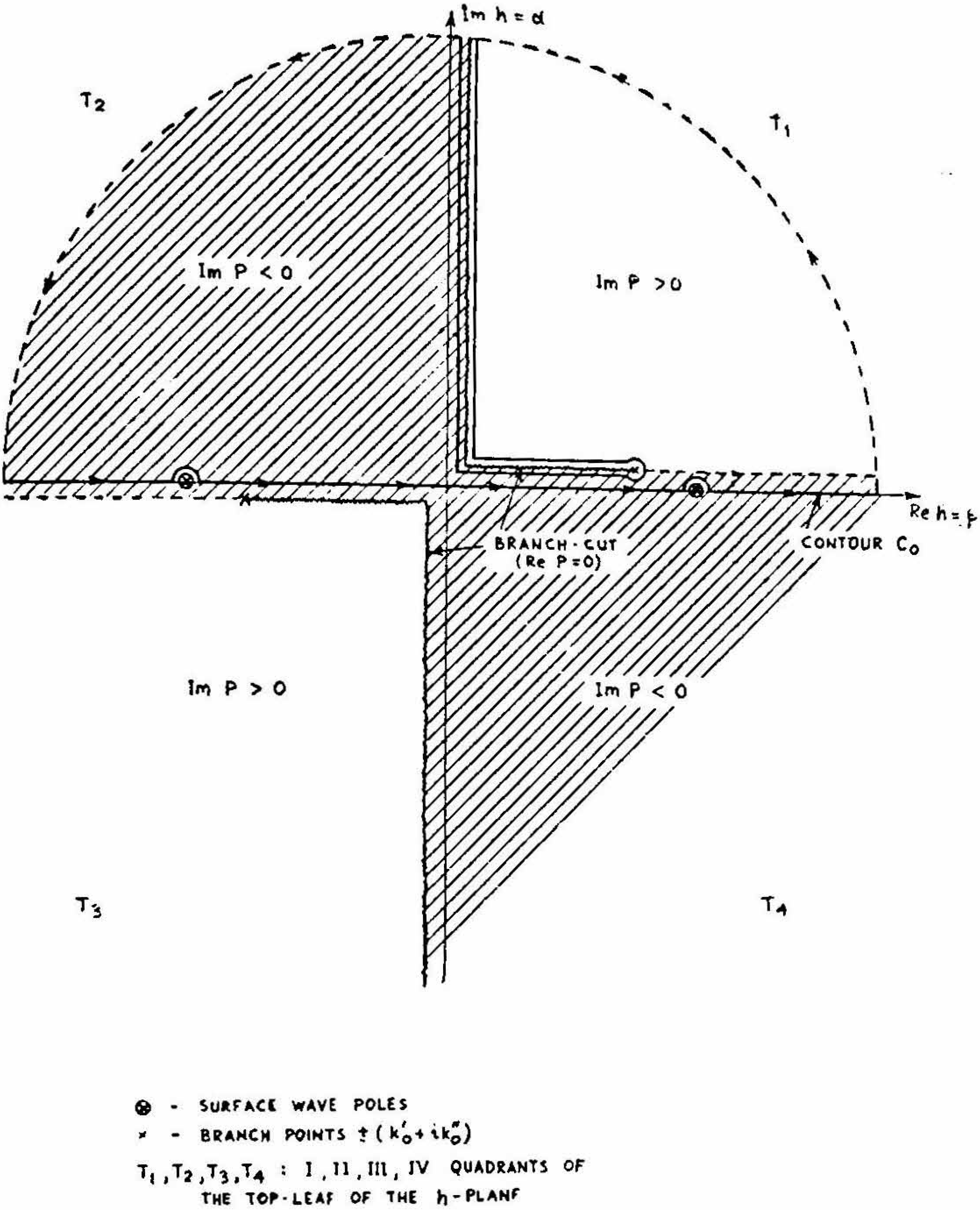


FIG. 9. Top leaf of the $h$-plane.

the integral (equation 23) transforms to

$$E_y = \int_{\mp\infty}^{\infty} F(\tau) \exp\{ik_0 r \cos(\tau - \theta)\}\, d\tau \tag{33}$$

in the $\tau$-plane where,

$$F(\tau) = \frac{k_0 q(\tau) \cos \tau}{\pi x(\tau)}.$$

The real and imaginary parts of $h$ and $p$ are

$$Re\, h = k_0 \sin \xi \cosh \eta \qquad (a)$$

$$Im\, h = k_0 \cos \xi \sinh \eta \qquad (b)$$

$$Re\, p = - k_0 \sin \xi \sinh \eta \qquad (= x) \qquad (c)$$

$$Im\, p = - k_0 \cos \xi \cosh \eta \qquad (= y) \qquad (d)$$

(34)

The four quadrants of the top leaf map onto the infinite strips $T_1$, $T_2$, $T_3$, $T_4$ and the four quadrants of the bottom leaf map onto the strips $B_1$, $B_2$, $B_3$, $B_4$ respectively (Fig. 10).

The function $f(\tau)$ in the index of the exponential function in the integrand, has a saddle-point at $\tau = \theta$ for

$$\frac{d}{d\tau} f(\tau) = \frac{d}{d\tau} \{ik_0 r \cos(\tau - \theta)\} = 0 \quad \text{at} \quad \tau = \theta.$$

So $f(\tau)$ can be expanded in Taylor's series around $\tau = \theta$ as

$$f(\tau) \cong f(\theta) + \frac{(\tau - \theta)^2}{2!} f''(\theta) + \ldots$$

$$\cong ik_0 r - ik_0 r \frac{(\tau - \theta)^2}{2}$$

neglecting the higher order terms when $\tau - \theta$ is small. Hence,

$$f(\tau) - f(\theta) = f_1 + if_2 = \frac{- ik_0 r \rho^2}{2} \exp(2i\omega)$$

which leads to

$$Re\,[f(\tau) - f(\theta)] = f_1 = \frac{- k_0 r \rho^2}{2} \sin 2\omega = \text{constant}$$

$$Im\,[f(\tau) - f(\theta)] = f_2 = \frac{- k_0 r \rho^2}{2} \cos 2\omega \text{ constant} \qquad (35)$$

where

$$\tau - \theta = \rho \exp(i\omega).$$

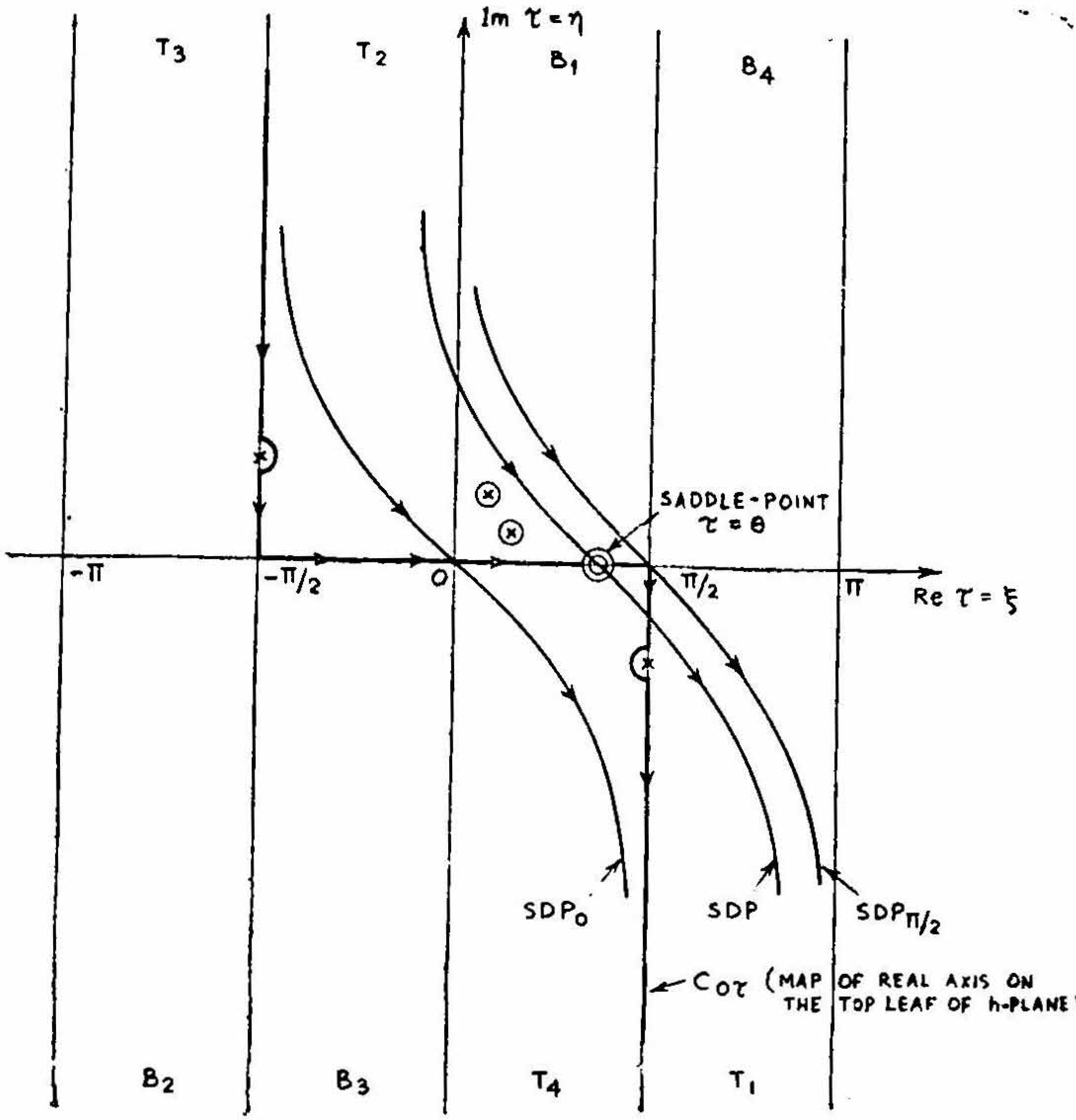


⊗ - COMPLEX POLES GIVING RISE TO LEAKY WAVES

× - SURFACE WAVE POLES

$T_1, T_2, T_3, T_4$ : MAPS OF I, II, III, IV QUADRANTS OF THE TOP LEAF OF h-PLANE

$B_1, B_2, B_3, B_4$ : MAPS OF I, II, III, IV QUADRANTS OF THE BOTTOM LEAF OF h-PLANE.

FIG. 10. Contours and poles in the $\tau$-plane.

The surface formed by the family of curves (equation 35) is in the form of a saddle (Fig. 11). On this surface the curves $f_2 = 0$ will be those along which the value of $f_1$ varies most rapidly and decreases when

$$\omega = \frac{-\pi}{4}, \frac{3\pi}{4},$$

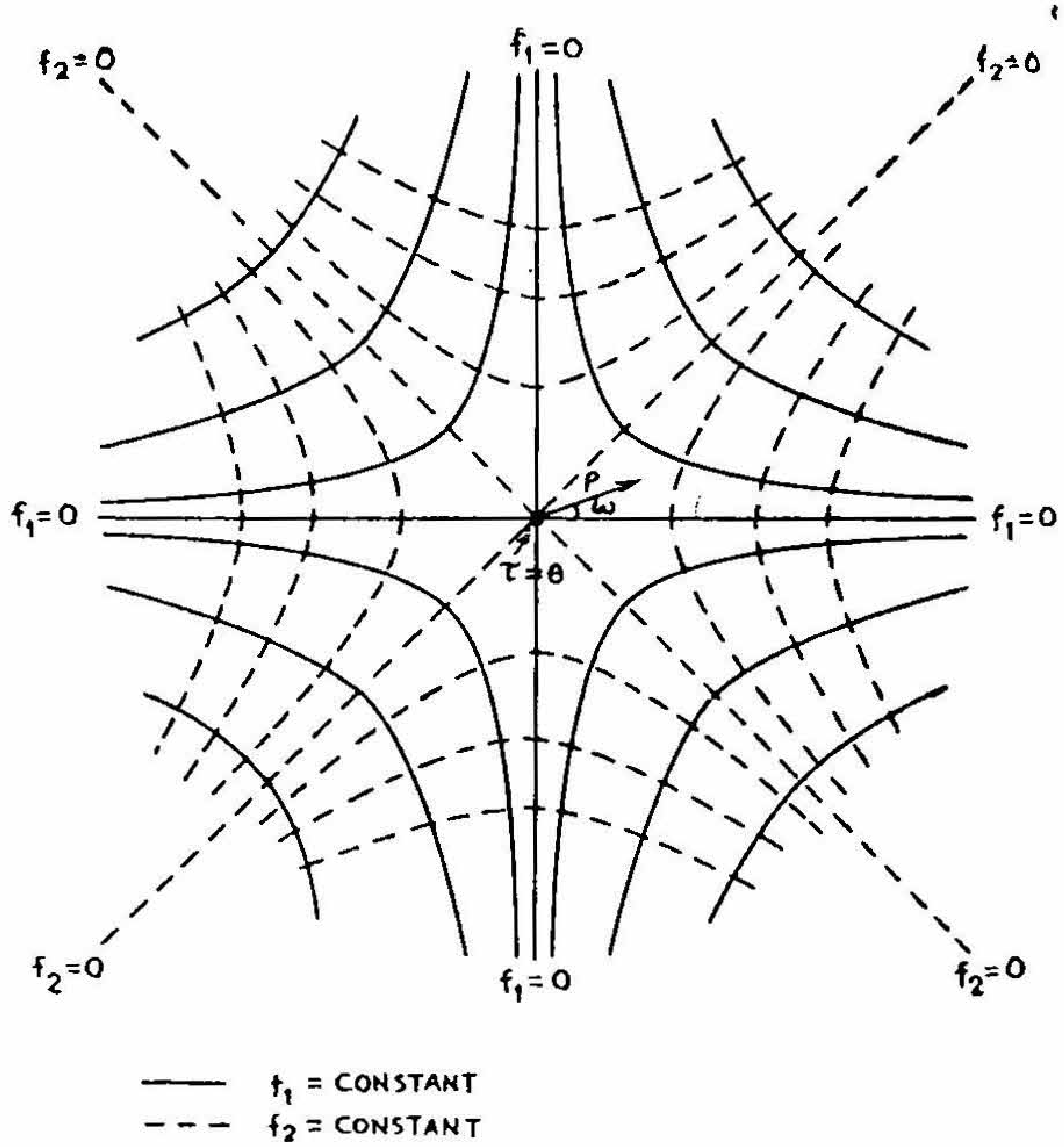


FIG. 11. Plot of $f_1$ = constant and $f_2$ = constant around the saddle point $\tau = \theta$.

and increases when

$$\omega = \frac{\pi}{4}, \frac{5\pi}{4}.$$

So, along the curve $f_2 = 0$ with $\omega = -\pi/4$ and $3\pi/4$, the expression $f(\tau) - f(\theta)$ decreases very rapidly from 0 to $-\infty$, on either side of the saddle point $\tau = \theta$, which is therefore the path of steepest discent (SDP).

If the contour $C_{0\tau}$ (Fig. 10) on the $\tau$-plane is deformed into *SDP* defined by $[f(\tau) - f(\theta)] = k_0 r \rho^2 \sin 2\omega/2$, then $\exp\{ik_0 r \cos(\tau - \theta)\} = \exp\{ik_0 r$

$+f_1 + if_2\} = \exp\{ik_0r - k_0r\rho^2/2\}$ will decay very fast as $\rho$ increases on either side of the saddle-point along the *SDP*. Hence the infinite integral (equation 33) is approximated to

$$E_y \cong \int F(\tau) \exp\left(ik_0 r \cos(\tau - \theta)\right) d\tau$$

along $C_0$

$$= \int F(\tau) \exp\{ik_0 r \,.\, \cos(\tau - \theta)\}\, d\tau$$

along a short length of *SDP*, $+ 2\pi i \times \Sigma$ *Res.* at the poles included between $C_{0\tau}$ and the *SDP* $+ \pi i \Sigma$ *Res.* at the poles on *SDP*. (34)

Along the *SDP*

$$\tau - \theta = \rho \exp\left(i\frac{3\pi}{4}\right) = -\rho \exp\left(-i\frac{\pi}{4}\right)$$

in the second quadrant of the $(\rho - \omega)$ plane and

$$\tau - \theta = \rho \exp(-i\pi/4)$$

in the fourth quadrant of the $\rho - \omega$ plane.

Hence,

$$d\tau = -\exp\left(-i\frac{\pi}{4}\right) d\rho \text{ in the II quadrant}$$

$$d\tau = \exp\left(-i\frac{\pi}{4}\right) d\rho \text{ in the IV quadrant.}$$

Since

$$f(\tau) = ik_0 r \cos(\tau - \theta) \cong ik_0 r - k_0 r\rho^2/2$$

$$\int_{SDP} F(\tau) \exp\{ik_0 r \cos(\tau - \theta)\}\, d\tau$$

$$\cong -\int_{SDP} F(\tau) \exp\left(ik_0 r - k_0 r\rho^2/2 - i\frac{\pi}{4}\right) d\rho$$

$$+ \int_{SDP} F(\tau) \exp\left\{ik_0 r \frac{\rho^2}{2} - i\frac{\pi}{4}\right\} d\rho. \quad (35)$$

Assuming $k_0 r \gg 1$, $\exp(-k_0 r^2/2)$ is very small for small value of $\rho = \rho_1$ or large $k_0 r$ in the region $|\tau - \theta| \leq \rho_1$. Hence, assuming $F(\tau) \simeq F(\theta)$, equation (35) reduces to

$$\int_{SDP} F(\tau) \exp\{ik_0 r \cos(\tau - \theta)\}\, d\tau$$

$$\cong 2F(\theta) \exp\left(ik_0 r - i\frac{\pi}{4}\right) \int_0^{\rho_1} \exp\left(-k_0 r \frac{\rho^2}{2}\right) d\rho.$$

Since, the contribution to the integral when $\rho > \rho_1$ is small $\exp(-k_0 r\rho^2/2)$ becomes negligible when $\rho > \rho_1$ the integral $\int_0^{\rho_1}$ can be written as $\int_0^{\infty}$. Hence,

$$\int_{SDP} = 2F(\theta) \exp\left(ik_0 r - i\frac{\pi}{4}\right)\left(\frac{2}{k_0 r}\right)^{\frac{1}{2}} \int_0^{\infty} \exp(-t^2)\, dt$$

$$= F(\theta) \exp\left(ik_0 r - i\frac{\pi}{4}\right)\left(\frac{2\pi}{k_0 r}\right)^{\frac{1}{2}} \tag{36}$$

where

$$t^2 = k_0 r \rho^2/2$$

and

$$\int_0^{\infty} \exp(-t^2)\, dt = \frac{1}{2}\Gamma\left(\frac{1}{2}\right) - \frac{\pi^{\frac{1}{2}}}{2}.$$

Equation (36) holds good provided there is no pole of $F(\tau)$ in the vicinity of the saddle point $\tau = \theta$. If there is a pole of $F(\tau)$ near the saddle-point, the approximation $F(\tau) \cong F(\theta)$ made in deriving equation (36) is not valid It is then necessary to use the modified saddle-point method [18].

By using Laurent's expansion, $F(\tau)$ can be written as

$$F(\tau) = G(\tau) + A/(\tau - \tau_0)$$

in the vicinity of the pole of $F(\tau)$, provided $\tau_0$ is a pole of first order. The poles of $F(\tau)$ used in the evaluation are all of first order. $G(\tau)$ is an analytic function of $\tau$ and $A$ the residue of $F(\tau)$ at $\tau = \tau_0$. Hence

$$\int_{SDP} F(\tau) \exp\{ik_0 r \cos(\tau - \theta)\}\, d\tau$$

$$= \int_{SDP} G(\tau) \exp\{ik_0 r \cos(\tau - \theta)\}\, d\tau$$

$$+ \int_{SDP} \frac{A}{\tau - \tau_0} \exp\{ik_0 r \cos(\tau - \theta)\}\, d\tau. \quad (37)$$

The first term in equation (37), evaluated by the ordinary saddle-point method yields

$$\int_{SDP} G(\tau) \exp\{ik_0 r \cos(\tau - \theta)\, d\tau$$

$$\cong G(\theta) \exp(ik_0 r - i\pi/4) \left(\frac{2\pi}{k_0 r}\right)^{\frac{1}{2}}$$

where

$$G(\theta) = -F(\theta) - A/(\theta - \tau_0).$$

Whereas, the second term

$$\int_{SDP} \frac{A}{\tau - \tau_0} \exp\{ik_0 r \cos(\tau - \theta)\}\, d\tau$$

$$\cong \int_{\rho_1}^{0} \frac{A}{\left(-\rho \exp\left(-i\frac{\pi}{4}\right) - \tau_0 + \theta\right)}$$

$$\times \exp\left(ik_0 r - i\frac{\pi}{4} - \frac{k_0 r \rho^2}{2}\right) d\rho$$

$$+ \int_{0}^{\rho_1} \frac{A}{\left(\rho \exp\left(-i\left(\frac{\pi}{4}\right) - \tau_0 + \theta\right)\right.}$$

$$\times \exp\left(ik_0 r - i\frac{\pi}{4} - \frac{k_0 r \rho^2}{2}\right) d\rho$$

$$= \int_{0}^{\rho_1} A \exp(ik_0 r - k_0 r/2)\, \frac{2(\tau_0 - \theta) \exp(i\pi/4)}{\rho^2 - i(\tau_0 - \theta)^2}\, d\rho.$$

As the value of the integrand is negligible when,

$$\int_{SDP} \frac{A}{\tau - \tau_0} \exp\{ik_0 r \cos(\tau - \theta)\}\, d\tau$$

$$\cong 2A \exp(ik_0 r + i\pi/4)(\tau_0 - \theta) \frac{1}{2} \int_0^\infty \frac{\exp(-k_0 r t/2)}{t^{\frac{1}{2}}\{t - i(\tau_0 - \theta)^2\}} dt$$

$$= i\pi A \exp[ik_0 r\{i - (\tau_0 - \theta)^2/2] \, erfc \left\{\exp\left(-i\frac{\pi}{4}\right)\right.$$

$$\left. \times (\tau_0 - \theta)\left(\frac{k_0 r}{2}\right)^{\frac{1}{2}}\right\}. \tag{38}$$

Since

$$\int_0^\infty \frac{\exp(-pt)}{t^{\frac{1}{2}}(t + a)} dt = \pi (a)^{-\frac{1}{2}} \exp(ap)\, erfc(a^{\frac{1}{2}} p^{\frac{1}{2}});$$

where

$$\rho^2 = t \quad \text{and} \quad erfc(z) = \int_z^\infty \exp(-t^2)\, dt.$$

The result (equation 38) is valid when the following inequality is satisfied.

$$-\pi < arg\{-i(\tau_0 - \theta)^2\} < \pi$$

*i.e.*,

$$-\frac{\pi}{4} < arg(\tau_0 - \theta) < 3\pi/4.$$

Otherwise

$$\int_{SDP} \frac{A}{\tau - \tau_0} \exp\{ik_0 r \cos(\tau - \theta)\, d\tau$$

$$= -i\pi A \exp[ik_0 r\{i - (\tau_0 - \theta)^2/2\}]$$

$$\times Erfc\left[\exp(-i\pi/4)(\theta - \tau_0)\left(\frac{k_0 r}{2}\right)^{\frac{1}{2}}\right] \tag{39}$$

when

$$-\frac{\pi}{4} < arg\,(\theta - \tau_0) < \frac{3\tau}{4}$$

or

$$\frac{3\pi}{4} < arg\,(\tau_0 - \theta) < -\pi/4.$$

7.2. *The residues at the poles.*—The residues at the poles are given by

$$R = \frac{q\,(\tau_0)\,k_0 \cos \tau_0 \exp \{ik_0 r \cos (\tau_0 - \theta)\}}{\pi \left.\dfrac{dx}{d\tau}\right|_{\tau=\tau 0}}$$

where

$$\frac{dx}{d\tau} = \frac{dx}{dh}\frac{dh}{d\tau}$$

$$= [\exp (+ pa)\,(2/p + d)\,(h/q)\,\{(p + q)^2 \exp (+ qd)$$

$$+ (p - q)^2 \exp (- qd)\} + (ah/p) \exp (+ pa)$$

$$\times \{(q + p)^2 \exp (+ qd) - (p - q)^2 \exp (- qd)\}$$

$$+ (ah/p)\, b^2 \exp (- pa)\, \{\exp (+ qd) - \exp (- qd)\}$$

$$- (dh/q)\, b^2 \exp (- pa)\, \{\exp (+ qd) + \exp (- qd)\}]$$

$$\times k_0 \cos \tau. \tag{40}$$

The residue can therefore be written as

$$R = P\,(\tau_0) \exp (ik_0 r) \cos (\tau_0 - \theta) \tag{41}$$

where

$$P\,(\tau_0) = [k_0 \cos \tau_0\, q\,(\tau_0)]/\pi \left.\frac{dx}{d\tau}\right|_{\tau=\tau 0}$$

$$h = k_0 \sin \tau$$

$$p = - ik_0 \cos \tau$$

$$q = [k_0^2 \sin^2 \tau - k^2]^{\frac{1}{2}}$$

$$\tau_0 = \xi_0 + iy_0$$

$$b^2 = k^2 - k_0^2.$$

since, the residues occur either as $i\pi R$ or $2i\pi R$, the value of $\pi P(\tau_0)$ has been calculated at some of the roots (Table III).

TABLE III

*Values of* $\pi P(\tau_0)$ *for poles used in the evaluation of the field*

$d = 0\cdot 0064/\text{m}$, $k_0 = 200$ rad/m, $k = 320$ rad/m

| *Rep* $x$ | *Imp* $y$ | *Re*$\tau_0$ $\xi$ | *Im*$\tau_0$ $\eta_0$ | *Re*$\pi P(\tau_0)$ | *Im*$\pi P(\tau_0)$ |
|---|---|---|---|---|---|
| − 1·363 | − 51·88 | 0·7107 | 0·07051 | 0·03349 | − 0·003796 |
| − 9·207 | − 151·959 | 1·3083 | 0·007057 | − 0·008635 | 0·0005631 |
| 149·35 | 0 | $\pi/2$ | − 0·6905 | 0·007364 | 0 |
| for $a = 0\cdot 00$ m and | | | | | |
| − 4·1865 | − 76·726 | 1·1772 | 0·02266 | − 0·01902 | 0·002513 |
| 149·5 | 0 | $\pi/2$ | − 0·6912 | 0·003246 | 0 |

The residue at a pole is taken into account only after the pole is included between the *SDP* and $C_0$, or in other words, there is a critical value of $\theta = \theta_c$ such that the residue is to be taken into account after the *SDP* crosses $\theta_c$ (Fig. 10).

7.3. *Complex poles in the strip* $B_1$ *on the* $\tau$ *plane.*—A complex pole in $B_1$, $\tau_0 = \xi_0 + i\,0\cdot 2$ (the value of $\eta_0 = 0\cdot 2$ is determined by trial) is captured, when

$$\theta - \xi_0 \geqslant \arccos(1/\cosh 0\cdot 2) = 11^\circ\, 18' \tag{42}$$

since $\theta$ should be greater than $\xi_0$ and the value of $\theta$ for which $(\xi_0, 0\cdot 2)$ satisfy the equation for *SDP* (Fig. 12) is given by $\cos(\xi_0 - \theta)\cosh 0\cdot 2 = 1$. The modulus of $R$ at $\tau_0$ satisfies the following condition;

$$\begin{aligned} |R| &= |P(\tau_0)\exp ik_0 r\cos(\tau_0 - \theta)| \\ &= |P(\tau_0)|\exp\{-ik_0 r\sin(\theta - \xi_0)\sinh 0\cdot 2\} \\ &\leq |P(\tau_0)|\exp(-8\cdot 04) \end{aligned} \tag{43}$$

for $r \geqslant 1$ meter and $(\theta - \xi_0)$ satisfying the inequality (42). Hence, the maximum value of the residues at $\tau_0 = \xi_0 + i\,0{\cdot}2$ is given by equation (43) for all values of $r$, $\theta$, the coordinates of the point of observation (Fig. 1). The maximum value of $|R|$ at a pole with $\eta$ even equal to $0{\cdot}2$ is very small. The value of $|R|$ is still smaller for poles whose $\eta < 0{\cdot}2$. So, the residue at the poles whose $\eta > 0{\cdot}2$ are negligible. Hence, even the largest value of residues at poles in the cross-hatched region (Fig. 12) are negligible. Only the complex poles in the dotted region of the strip $B_1$ therefore, need be considered.

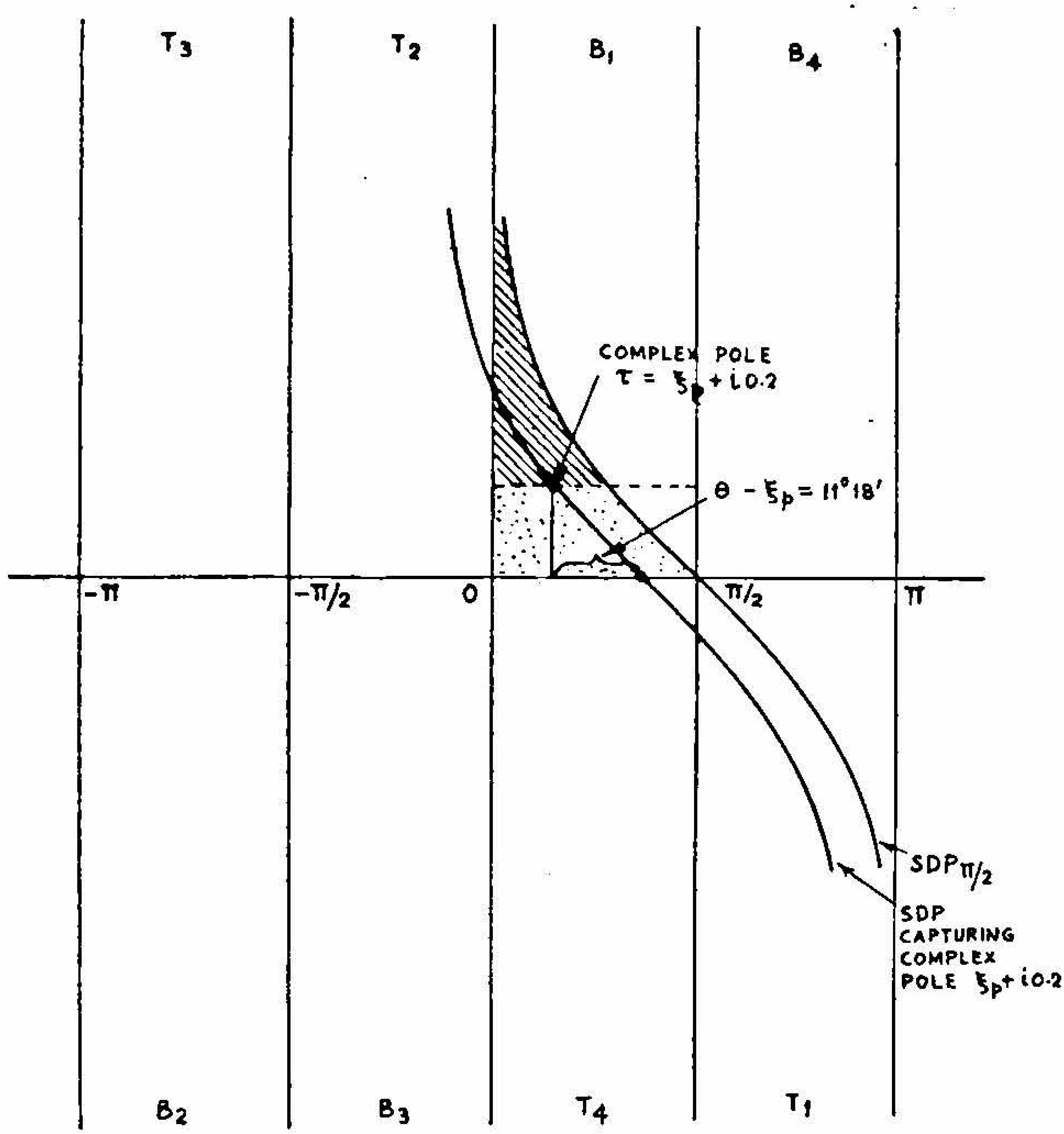


FIG. 12. Range of $\xi$ and $\eta$ in which complex poles in the strip $B_1$ have to be determined.

If the ranges of $\xi$ and $\eta$ in the dotted region (Fig. 12) are transformed according to equations (34 *c* and 34 *d*), the ranges of $x$ and $y$ in which the complex roots have to be found are $0 < x < -40$; $0 < y < -200$. In calculating the value of the residues, larger ranges were used, so that no significant poles was left out. Furthermore, an evaluation of $|F(\tau)|$ at discrete values of $\xi$ and $\eta$ in the dotted region of strip $B_1$ (Fig. 12) confirms the existence of complex roots, giving rise to leaky waves (Table I). The plots (Fig. 13) of $|F(\tau)|$ for values of $\xi$ in the range of 0° to 90° *i.e.*, $0 < \xi < \pi/2$ for fixed values of $\eta$ show that for $a = 0$ and $a = 0 \cdot 00365$ m, there are no complex roots in the dotted region of the strip $B_1$, which means that for these spacings between the two plates, there are no leaky waves contributing to the field at large distances from the source. Whereas, for $a = 0 \cdot 02$ m and $a = 0 \cdot 03$ m, there is one complex root at $\xi_0 \cong 67° = 1 \cdot 17$ and $\eta_0 \cong 0 \cdot 02$ and there are two complex roots at $\xi_{01} \cong 41° = 0 \cdot 7$, $\eta_{01} \cong 0 \cdot 07$, and $\xi_{01} \cong 75° = 31$, $\eta_{01} \cong 0 \cdot 01$ respectively in the dotted region of $B_1$.

7.4. *Numerical Evaluation of the field.*—The field is evaluated numerically by using the following expressions (Appendix A. 3)

$$E_y = \begin{cases} \exp(ik_0 r - i\pi/4)\, F(\theta) \left(\dfrac{2\pi}{k_0 r}\right)^{\frac{1}{2}} \\ \text{when} \\ \quad |\tau_{0i}' - \theta| > \epsilon_i & (44) \\ \exp(ik_0 r - i\pi/4)\, \{F(\theta) - A_{0i}'(\theta - \tau_{0i}')\} \left(\dfrac{2\pi}{k_0 r}\right)^{\frac{1}{2}} \\ \quad + i\pi A_{0i}' \exp[ik_0 r\{i - (\tau_{0i}' - \theta)^2/2\}] \\ \quad \times Erfc\left\{\exp(-i\pi/4)(\tau_{0i}' - \theta)\left(\dfrac{k_0 r}{2}\right)^{\frac{1}{2}}\right\} \\ \text{when} \\ \quad |\tau_{0i}' - \theta| < \epsilon_i \;\&\; -\dfrac{\pi}{4} < arg(\tau_{0i}' - \theta) < \dfrac{3\pi}{4} & (45) \\ \exp(ik_0 r - i\pi/4)\, \{F(\theta) - A_{0i}'/(\theta - \tau_{0i}')\} \left(\dfrac{2\pi}{k_0 r}\right)^{\frac{1}{2}} \\ \quad - i\pi A_{0i}' \exp[ik_0 r\{i - (\tau_{0i}' - \theta)^2/2\}] \\ \quad \times Erfc\left\{\exp(-i\pi/4)(\theta - \tau_{0i}')\left(\dfrac{k_0 r}{2}\right)^{\frac{1}{2}}\right\} & (46) \\ \text{when} \\ \quad |\tau_{0i}' - \theta| < \epsilon_i \;\&\; \dfrac{3\pi}{4} < arg(\tau_{0i}' - \theta) > -\pi/4 \end{cases}$$

where $\tau_0$ is a pole of $F(\tau)$ and $A$ is the residue at $\tau_0$.

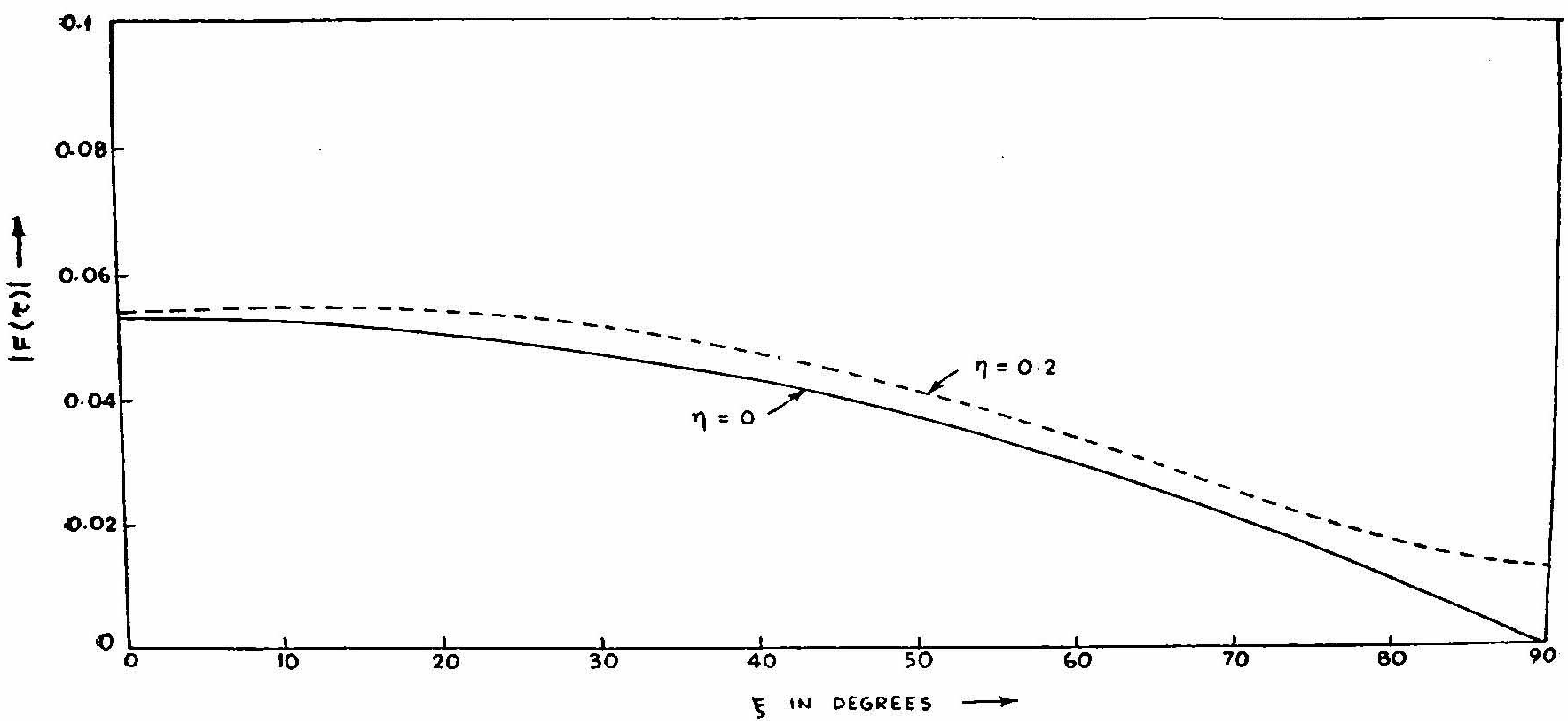


FIG. 13 (a). Plot of modulus F (τ) for values of $\xi$ between 0° and 90° (0 to $\pi/2$) for fixed $\eta$. $a = 0$ m, $d = 0{\cdot}0064$ m, $k_0 = 200$ radians per metre, $k = 320$ radians per metre.

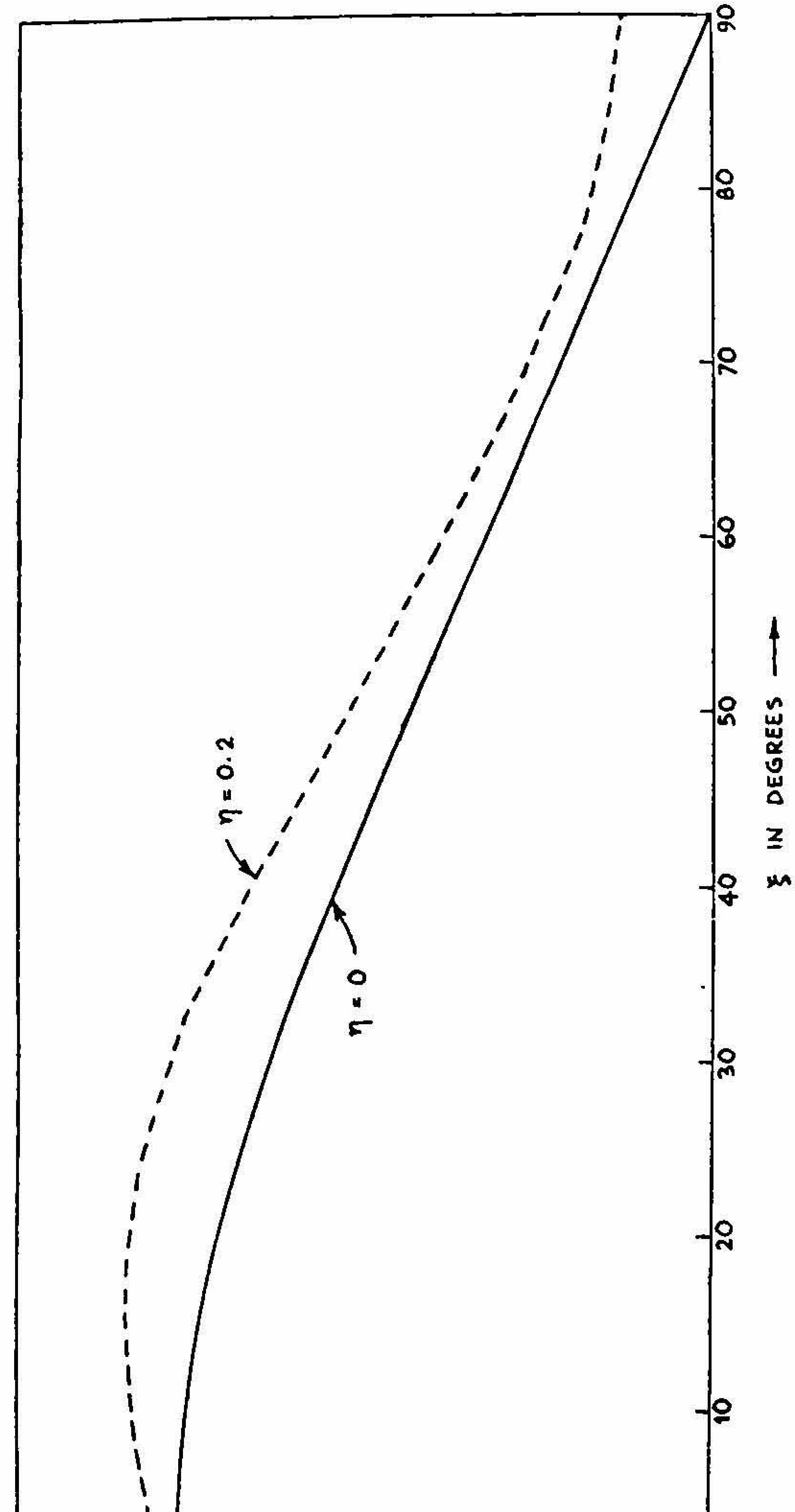


FIG. 13 (*b*). Plot of modulus of F(τ) *versus* ξ in degrees for fixed η. $a = 0{\cdot}00365$ m, $d = 0{\cdot}0064$ m, $k_0 = 200$ radians per metre, $k = 320$ radians per metre,

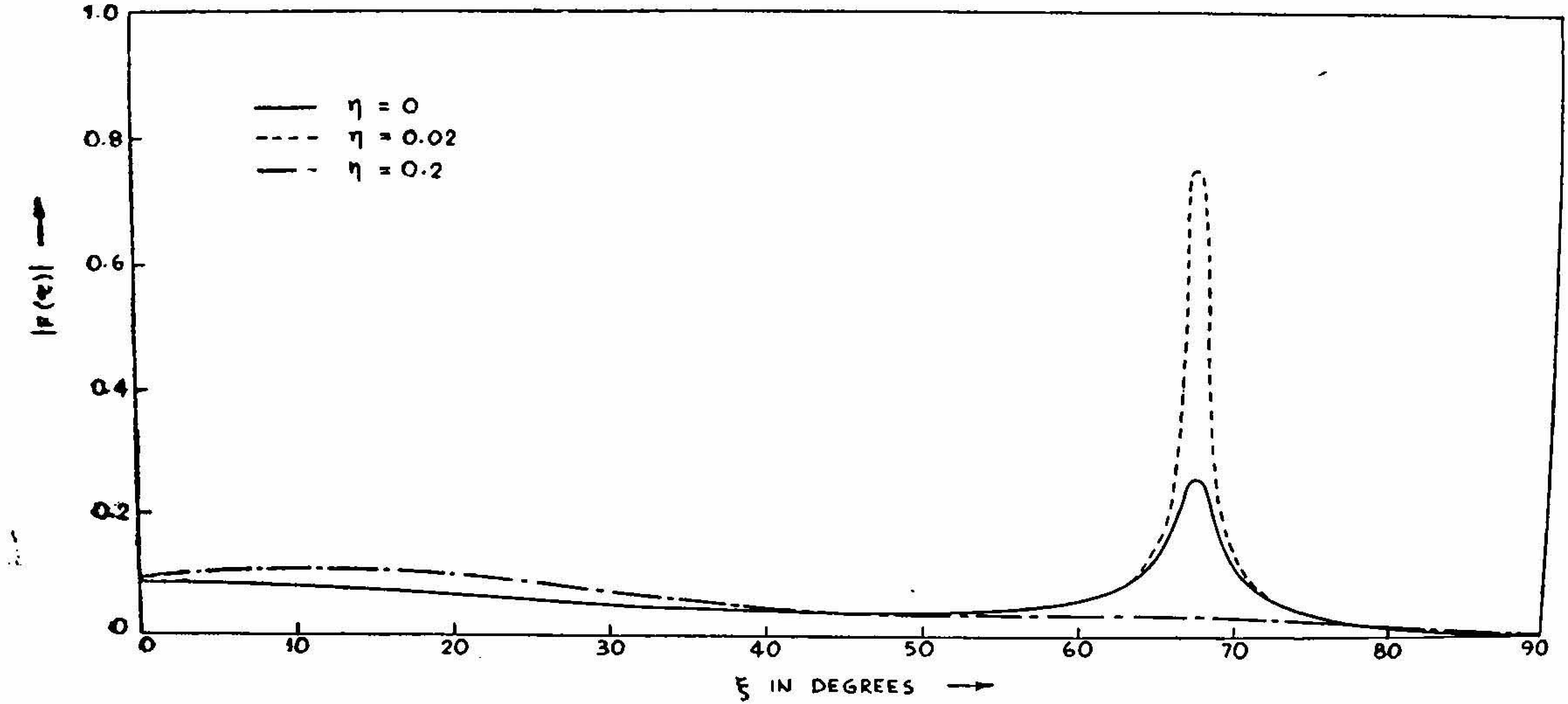


FIG. 13 (*c*). Plot of modulus of F($\tau$) *versus* $\xi$ in degrees for fixed $\eta$. $a = 0 \cdot 02$ m, $d = 0 \cdot 0064$ m, $k_0 = 200$ radians per metre, $\kappa = 320$ radians per metre.

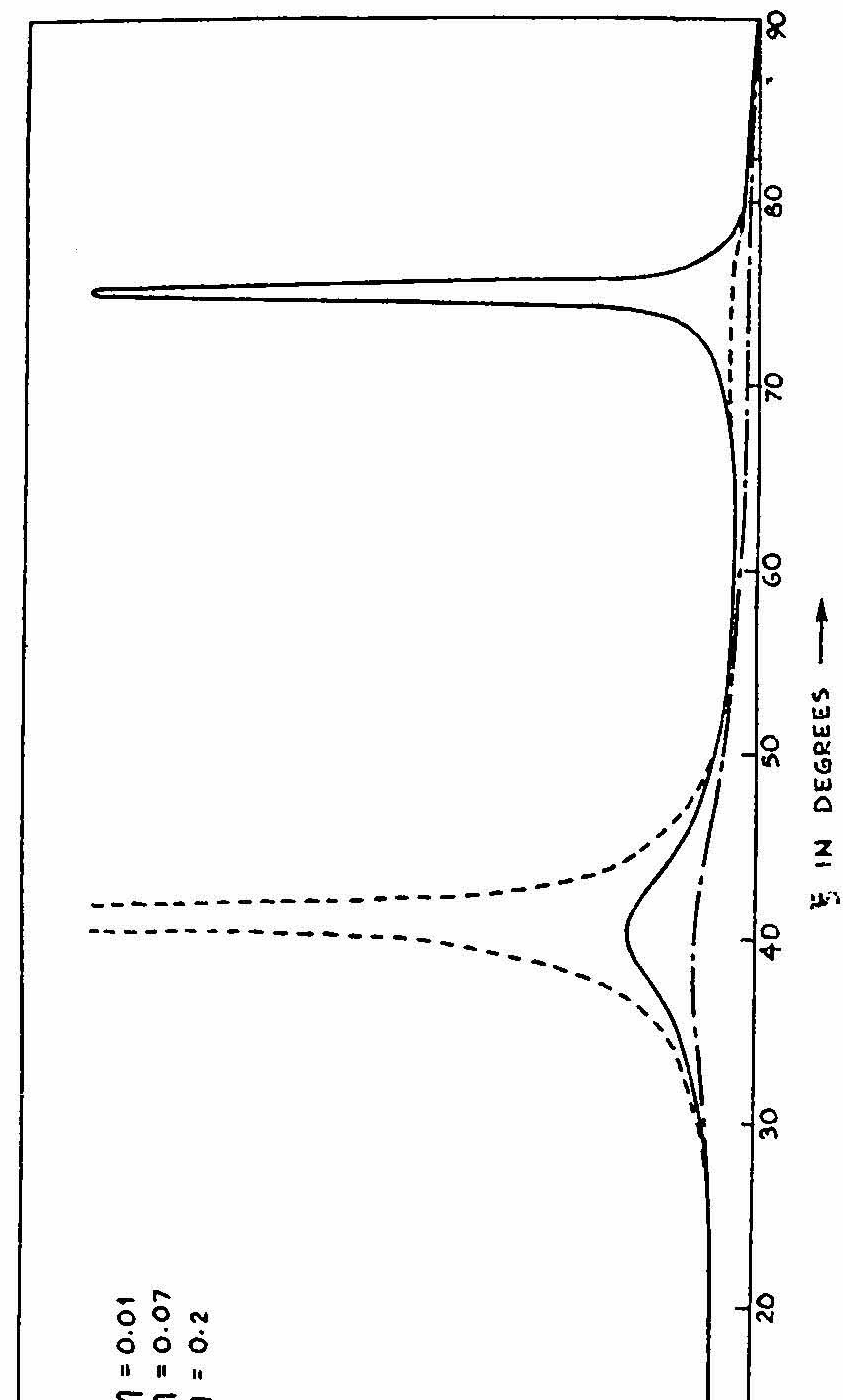


FIG. 13 (*d*). Plot of modulus of F (τ) *versus* ξ in degrees for fixed values of η, $a = 0{\cdot}03$ m, $d = 0{\cdot}0064$ m, $k_0 = 200$ radians per metre, $k = 320$ radians per metre.

In evaluating the field, the following poles are taken into account for $a = 0\cdot03$ m, $d = 0\cdot0064$ m, $k_0 = 200$ rad/m, $k = 320$ rad/m

(i) $\tau_{01} = \xi_{01} + i\eta_{01} = 0\cdot7107 + i\,0\cdot07051$

(ii) $\tau_{02} = \xi_{02} + i\eta_{02} = i\,0\cdot3083 + i\,0\cdot007057$
Res. at $\tau_{01}$ is $A_1 = 0\cdot01066 - i\,0\cdot0012085$
Res. at $\tau_{02}$ is $A_2 = 0\cdot002749 + i\,0\cdot0001793$.

When $\theta > \theta_{c1}$, where $\theta_{c1}$ is given by

$$\cos(\xi_{01} - \theta_{c1}) \cosh \eta_{01} = 1$$

*i.e.*,

$$\theta > \xi_{01} + \cos^{-1}(1/\cosh \eta_{01}) \cong 45°,$$

the term

$$2\pi i A_1 \exp\{ik_0 r \cos(\tau_{01} - \theta)\}$$

is to be added to the sum of the residues. Whereas, if $\theta > \theta_{c2}$, where,

$$\theta_{c2} = \xi_{02} + \cos^{-1}(1 \cosh \eta_{02}) \cong 76°,$$

the term

$$2\pi i A_2 \exp\{ik_0 r \cos(\tau_{02} - \theta)\}$$

is to be added. The residue term $2\pi i\,(0\cdot0002344).\exp\{ik_0 r \cos(\pi/2 - i\,0\cdot6905 - \theta)\}$ of the surface wave pole $\tau_{s1} = \pi/2 - i\,0\cdot6905$ is to be added

when

$$\theta > \theta_c = \pi/2 + \cos^{-1}(1/\cosh 0\cdot6905) \cong 0\cdot93 \text{ rad.}$$

But for $a = 0\cdot02$ m and $d$, $k$, $k_0$ having the same values as above, the Res. at the complex pole $\tau_0 = \xi_0 + i\eta_0 = 1\cdot1772 + i\,0\cdot02266$ in $A_0 = -0\cdot006056 + 0\cdot0007999$. The term $2\pi i A_0 \{ik_0 r \cos(\tau_0 - \theta)$ is to be added when $\theta > \xi_0 + \cos^{-1}(1/\cosh \eta_0) = 69°$. The residue term $2\pi i\,(0\cdot001033)$ $\exp\{ik_0 r \cos(\pi/2 - 10\cdot6912 - \theta)$ at the surface wave pole $\tau_{s1}' = \pi/2 - i$ $0\cdot6912$ is added when $\theta > \pi/2 + \cos^{-1}$ $(1/\cosh 0\cdot6912) = 0\cdot93$ radian.

For smaller values of $a = 0\cdot00365$ and $a = 0m$, there are no significant complex poles and the field is evaluated by using equation (44). The roots associated with the surface waves are found by using equation 27. For $a = 0\cdot00365$ m, $2\pi i$ Res. at the surface wave pole $\tau_{s1}'' = \pi/2 - i\,0\cdot76$ is $i\,1\cdot8 \exp\{ik_0 r \cos(\pi/2 - i\,0\cdot76 - \theta)$ and for $a = 0$ m, $2\pi i$ Res. $= i\,1\cdot72$ $\exp\{ik_0 r \cos(\pi/2 - i\,0\cdot89 - \theta)$ at the surface wave pole $\tau_{s1}''' = \pi/2 - i$ $0\cdot89$. These residues are to be added to the field given by equation 44 when $\theta > 0\cdot78$ radian.

The plots of $|E_y|$ with respect to $x$, $z$, and $\theta$, (Figs. 14–16) show that

(i) For small values of spacing $|E_y|$ remains constant in the $z$-direction and the radiation field is less than 5·5% of the surface wave field on the guide surface. In the azimuthal direction for $\theta < \theta_c$, only the radiation field is predominant. As $\theta$ becomes greater than $\theta_c$ and approaches 90°, the surface wave field becomes predominant, and the decay of the field in the $x$-direction is the same as the decay of a surface wave. Moreover, as the total field consists of the space wave term given by $2\pi i$ X Res. at the complex pole on $\xi = \pi/2$ line, and the modulus of the space wave term for any $\theta$ is less than 5·5% of the value of the modulus of the surface wave term of $\theta = 90°$, so the surface wave term in this case is significant.

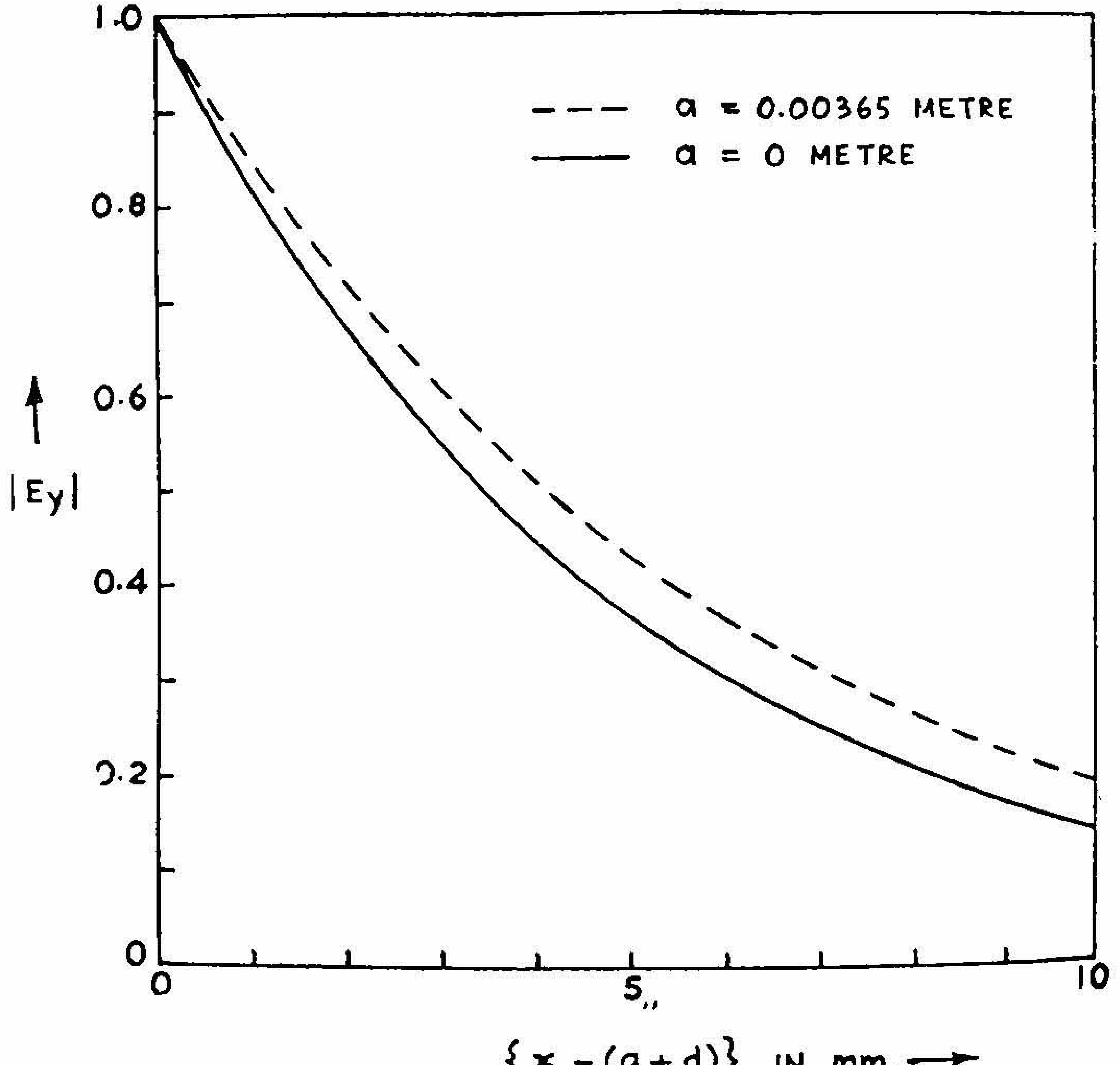


FIG. 14 (*a*). Theoretical decay of the normalised $|E_y|$ in the transverse direction. $d = 0·0064$ m, $k_1 = 200$ radians per metre, $k = 320$ radians per metre.

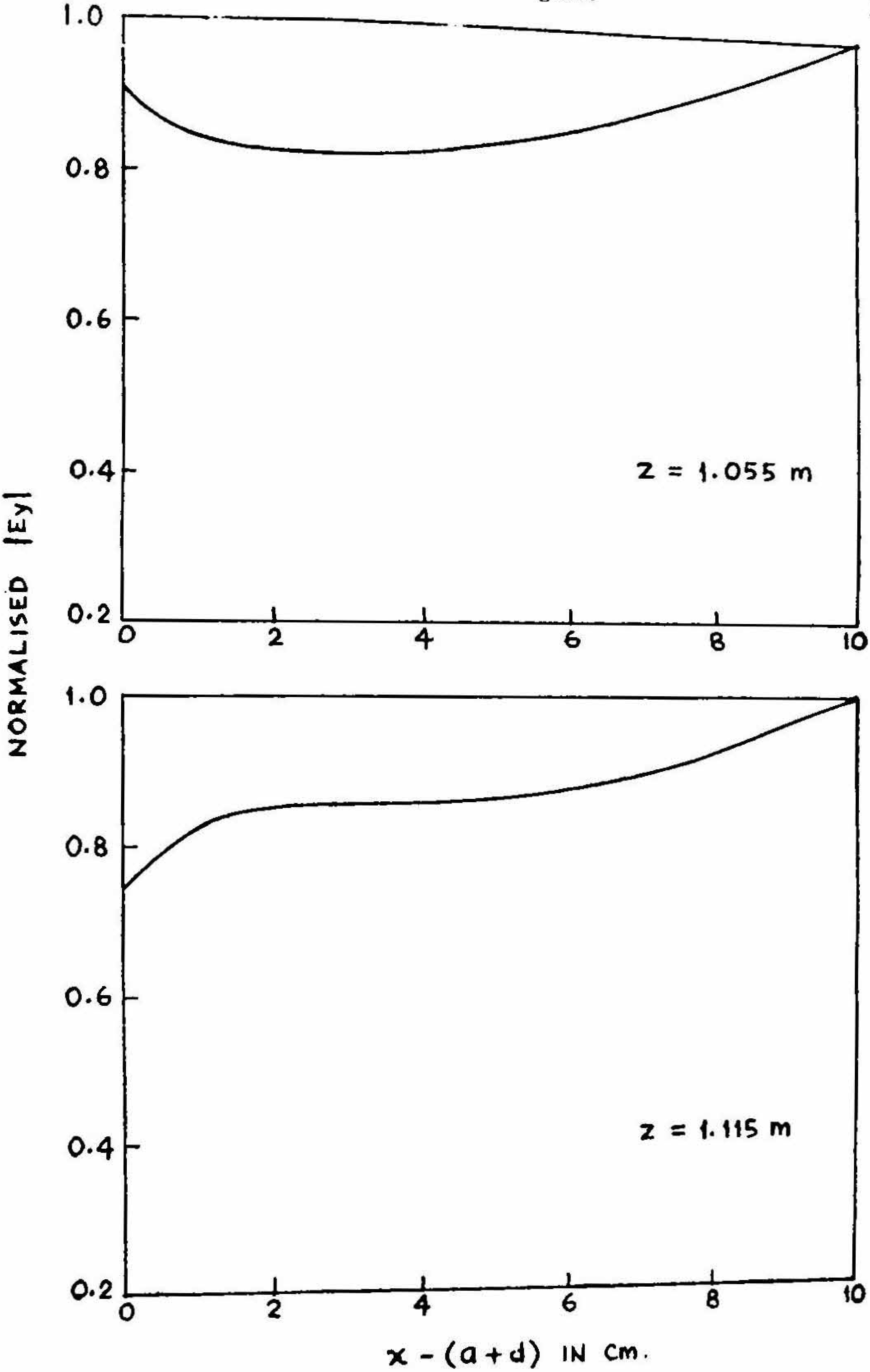


FIG. 14 (*b*). Plot of normalised modulus of $E_y$ versus $x-(a+d)$. $x-(a+d)=0$: Surface of the dielectric guide, $z=0$: Source, $a=0{\cdot}03$ m, $d=0{\cdot}0064$ m, $k_0=200$ radians per metre, $k=320$ radians per metre.

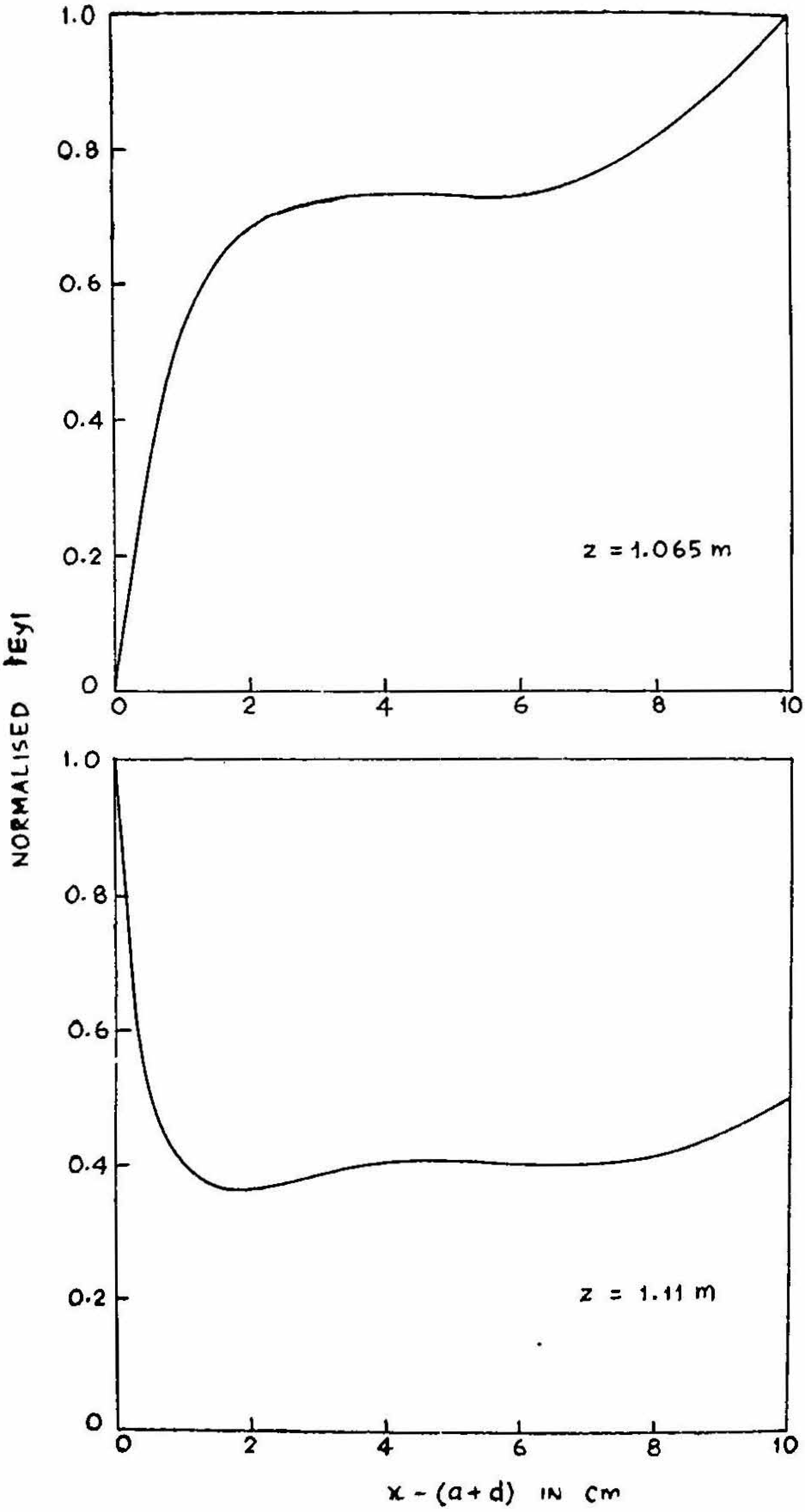


FIG. 14 (c). Plot of normalised modulus of $E_y$ versus $x - (a + d)$ for fixed $z$. $x - (a + d) = 0$: Surface of the dielectric guide, $z = 0$: Source, $a = 0{\cdot}02$ m, $d = 0{\cdot}0064$ m, $k_0 = 200$ radians per metre, $k = 320$ radians per metre.

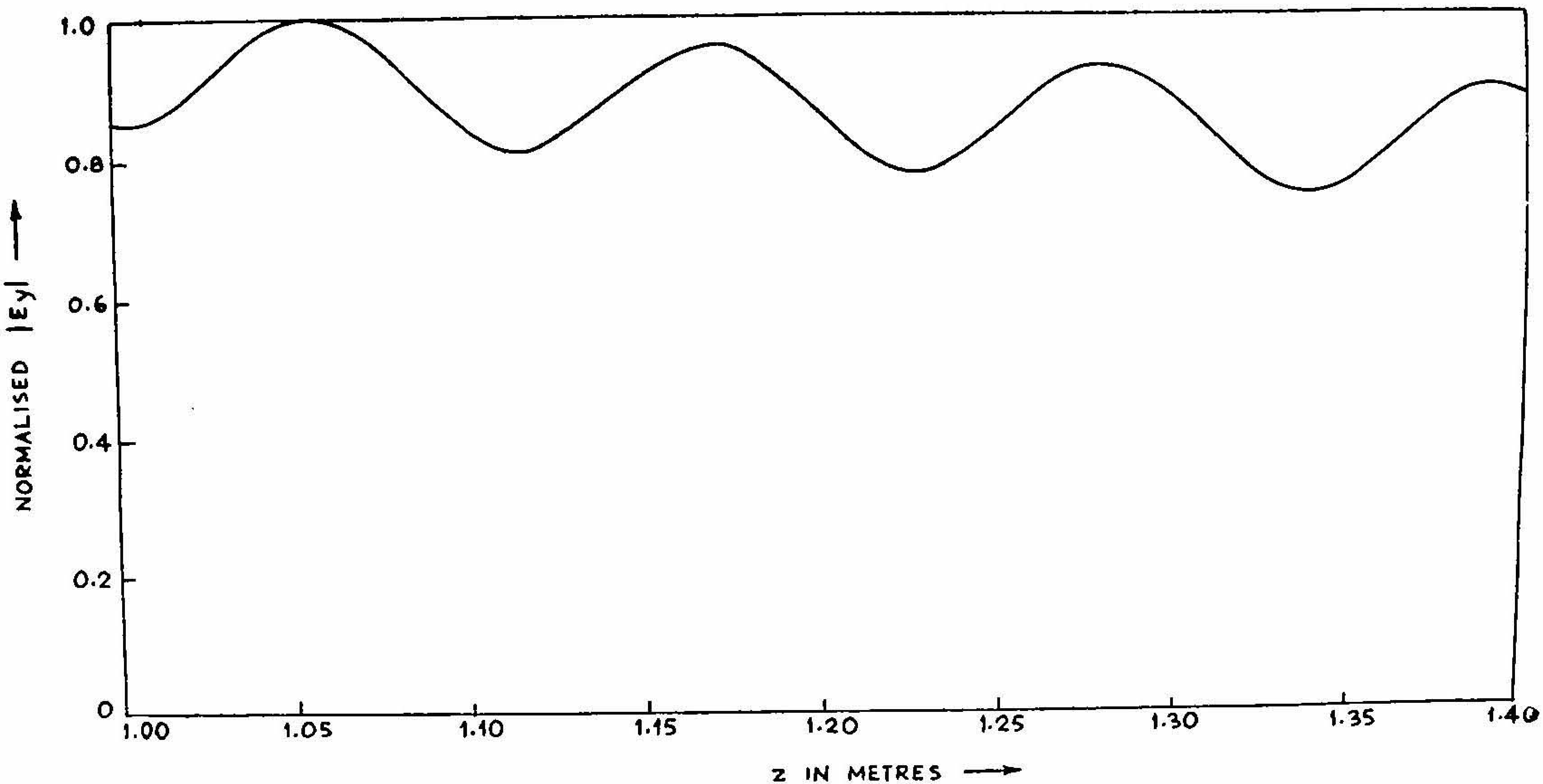


FIG. 15(*a*). Plot of normalised modulus of $E_y$ versus $z$. $z = 0$: Source, $a = 0{\cdot}03$ m, $d = 0{\cdot}0064$ m, $k_0 = 200$ radians per metre, $k = 320$ radians per metre.

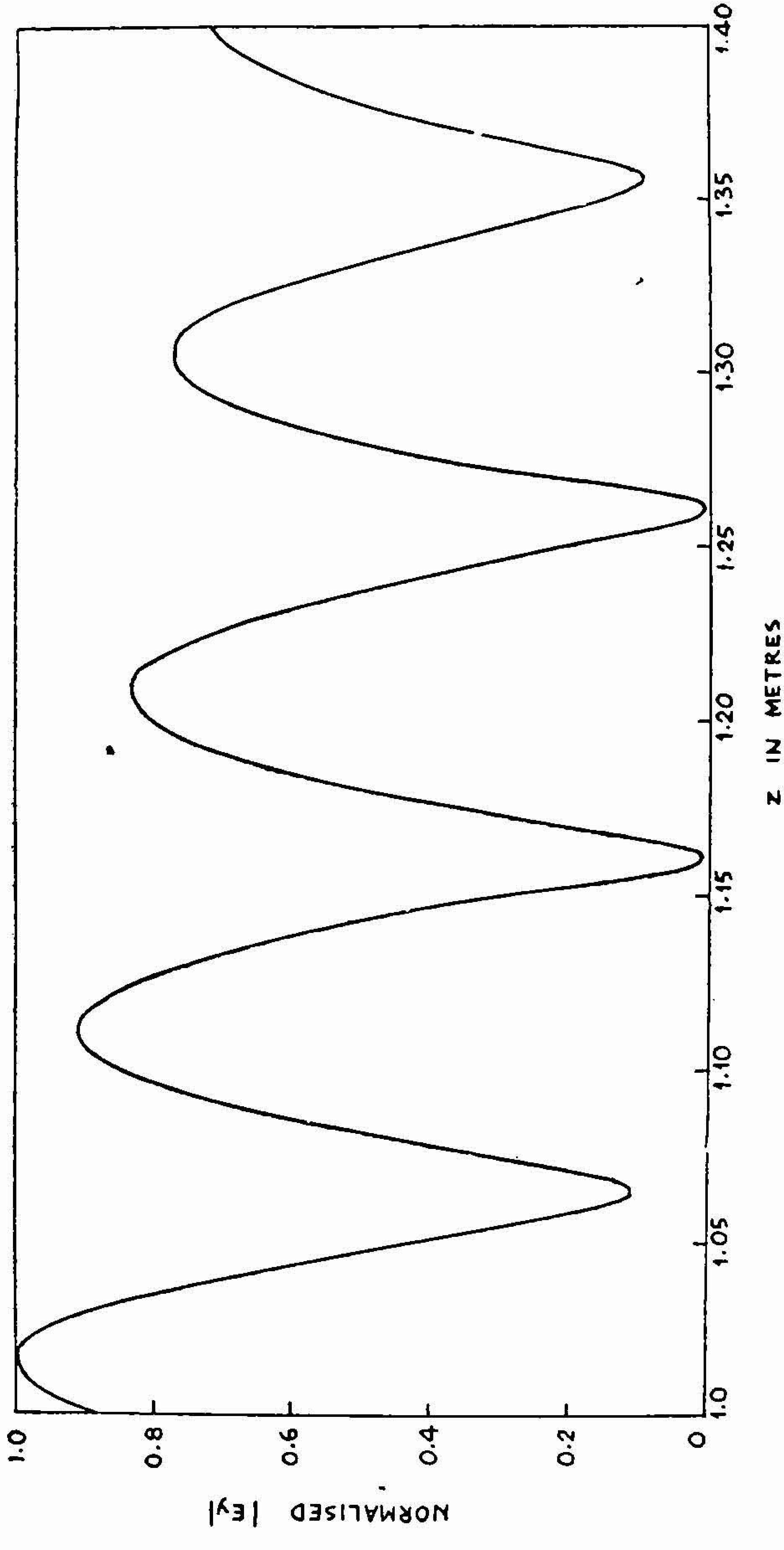


FIG. 15 (*b*). Plot of normalised modulus of $E_y$ versus $z$. $z = 0$: Souce, $a = 0{\cdot}02$ m, $d = 0{\cdot}0064$ m, $k_0 = 200$ radians per metre, $k = 320$ radians per metre.

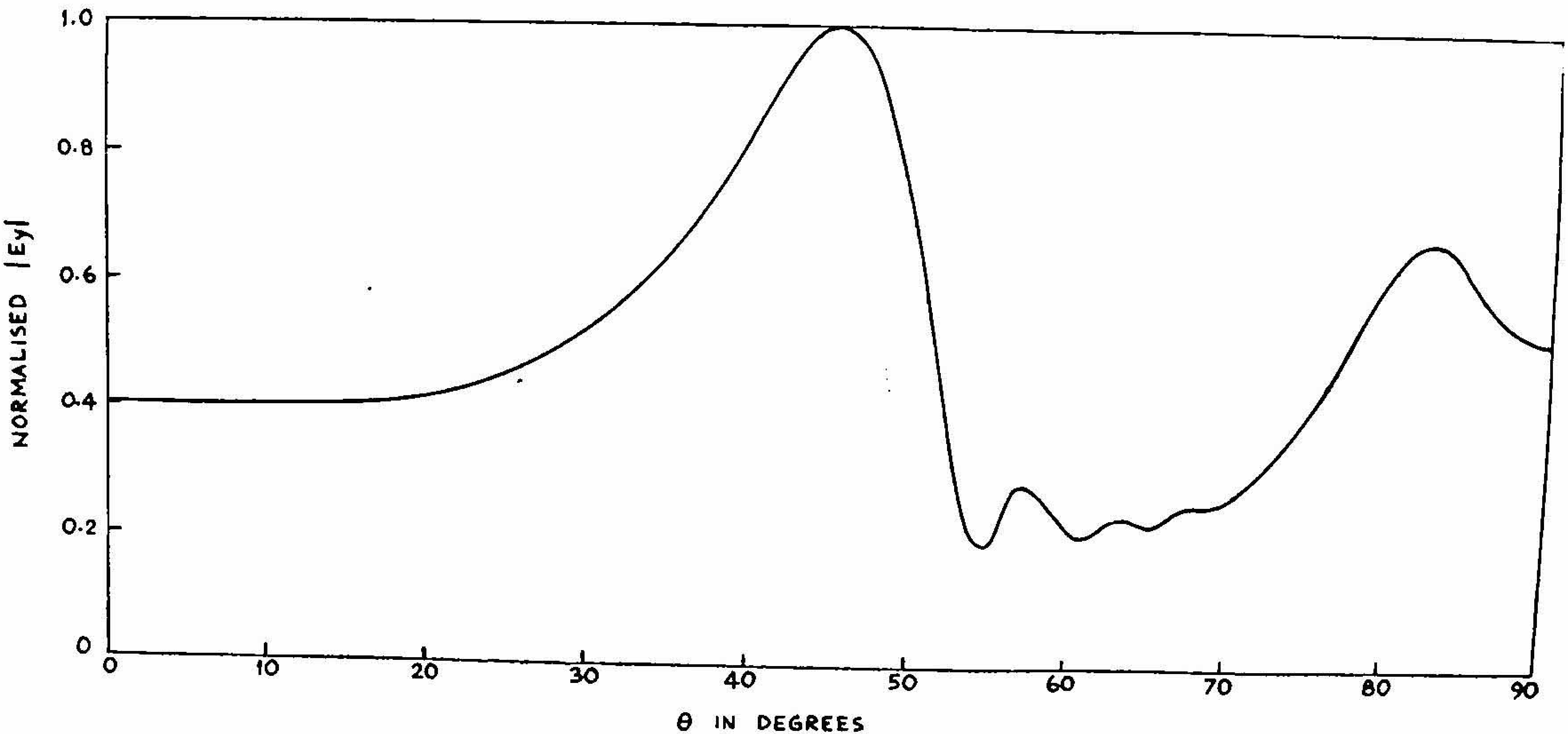


FIG. 16 (*a*). Plot of normalised modulus of $E_y$ versus $\theta$ for $r = 1$ metre. $a = 0{\cdot}03$ m, $d = 0{\cdot}0064$ m, $k_0 = 200$ radians per metre, $k = 320$ radians per metre.

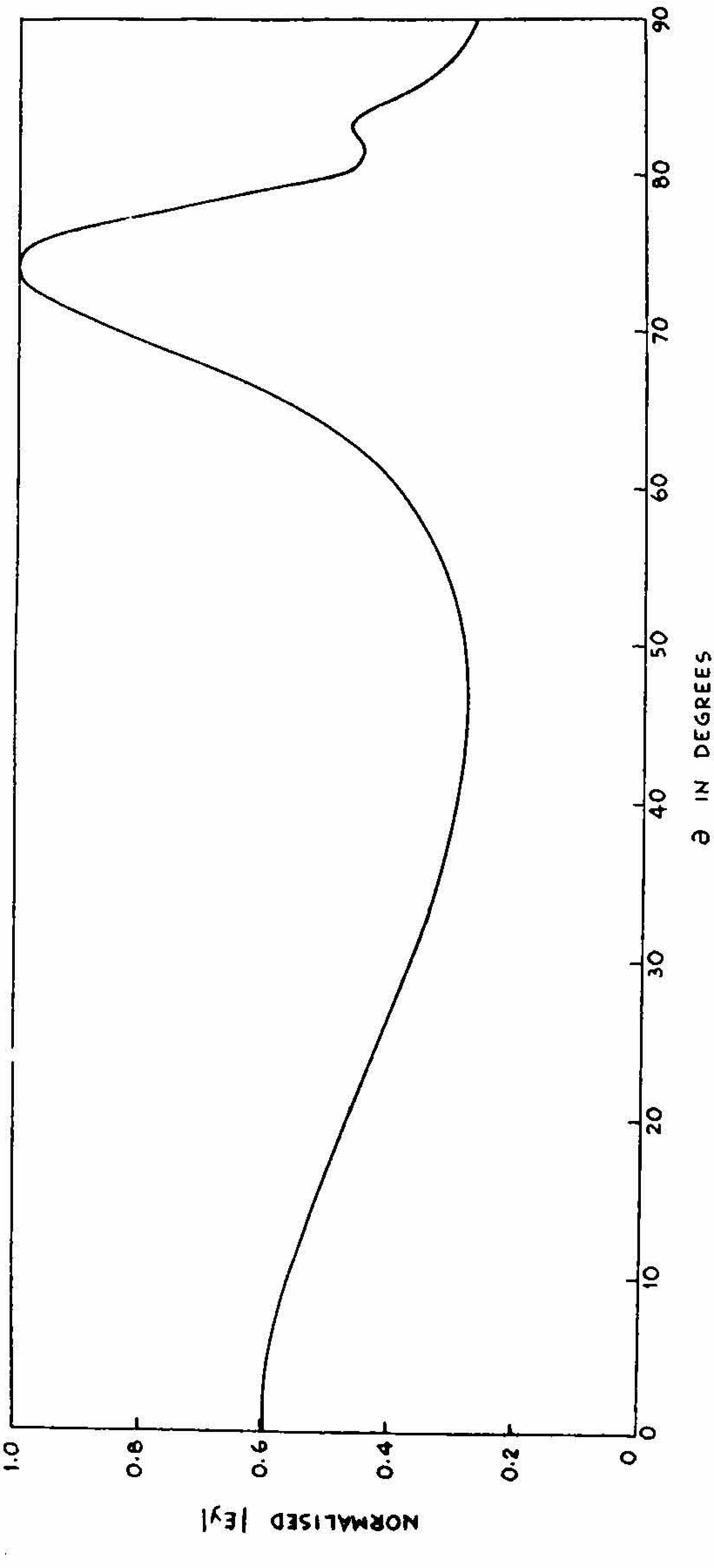


FIG. 16 (*b*). Plot of normalised modulus of $E_y$ versus $\theta$ for $r = 1$ metre. $a = 0{\cdot}02$ m, $d = 0{\cdot}0064$ m, $k_0 = 200$ radians per metre, $k = 320$ radians per metre.

(ii) In the case of larger spacing $a = 0 \cdot 02$ m and $a = 0 \cdot 03$ m, the variation of $| E_y |$ in the $z$ and $x$ directions is an interference pattern due to the superposition of the space wave, leaky wave and surface waves. In the azimuthal direction, the nature of the variation of $E_y$ depends on the magnitude of $\theta$. When $\theta$ is very small, the field corresponds to that obtained by the ordinary saddle-point method. When $\theta$ is close to the complex poles in $B_1$ strip, lobes appear at these values of $\theta$. The number of lobes corresponding to the number of complex poles. In the rest of the regions of $\theta$, the field shows interference pattern.

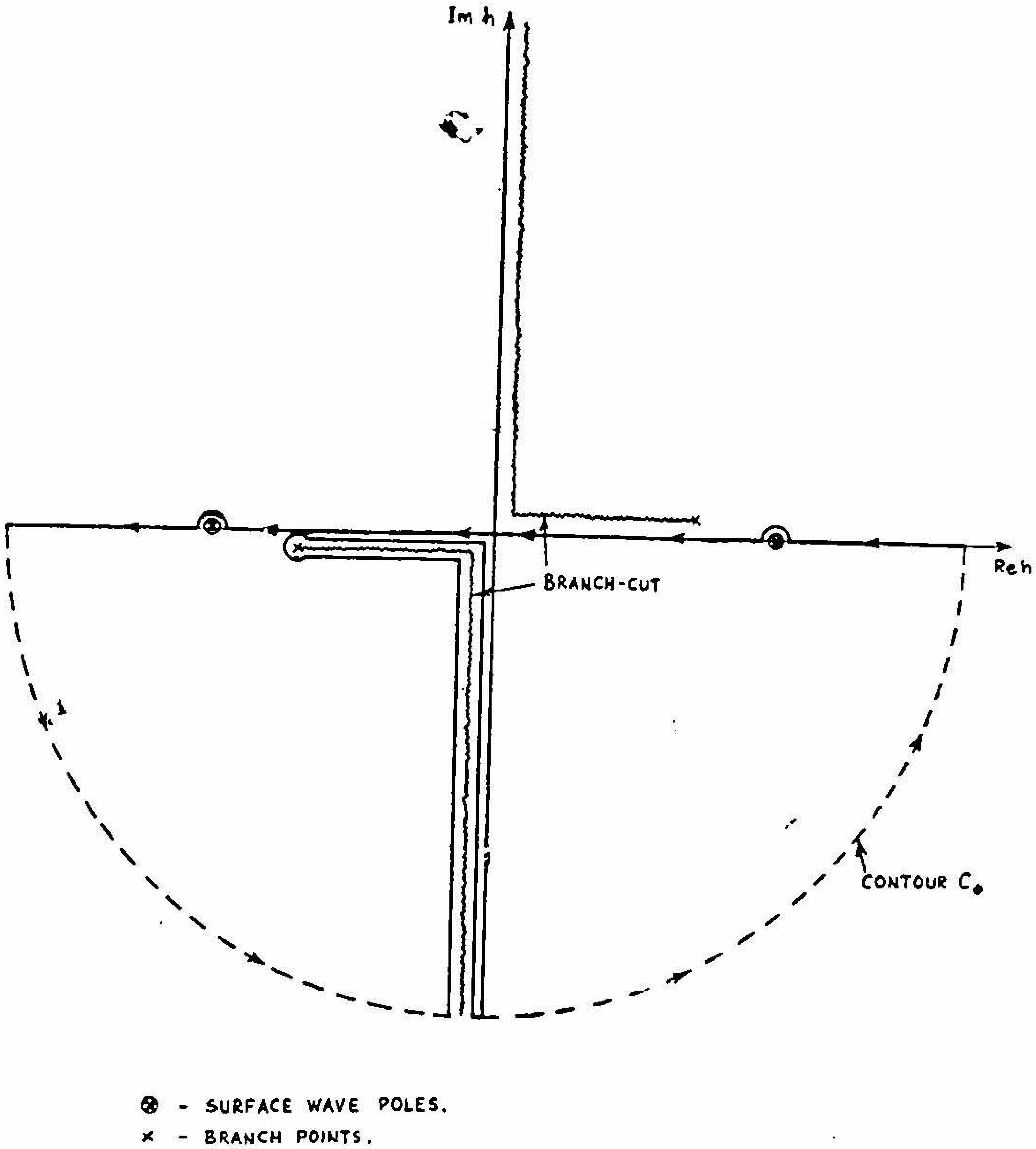


FIG. 17. Contour on the top leaf of the $h$-plane for the case of $z$ less than zero.

(iii) For $z < 0$, the integral giving the field is evaluated by using a contour in the bottom half of the top leaf of the $h$-plane. The negative values of $z$ and $h$ thus result in the same values of the field as when $z$ 0. The field outside the plates is

$$\int_{-\infty}^{\infty} \frac{q}{\pi x} \exp\left[-p\{x-(a+d)\}+ihz\right] dh$$

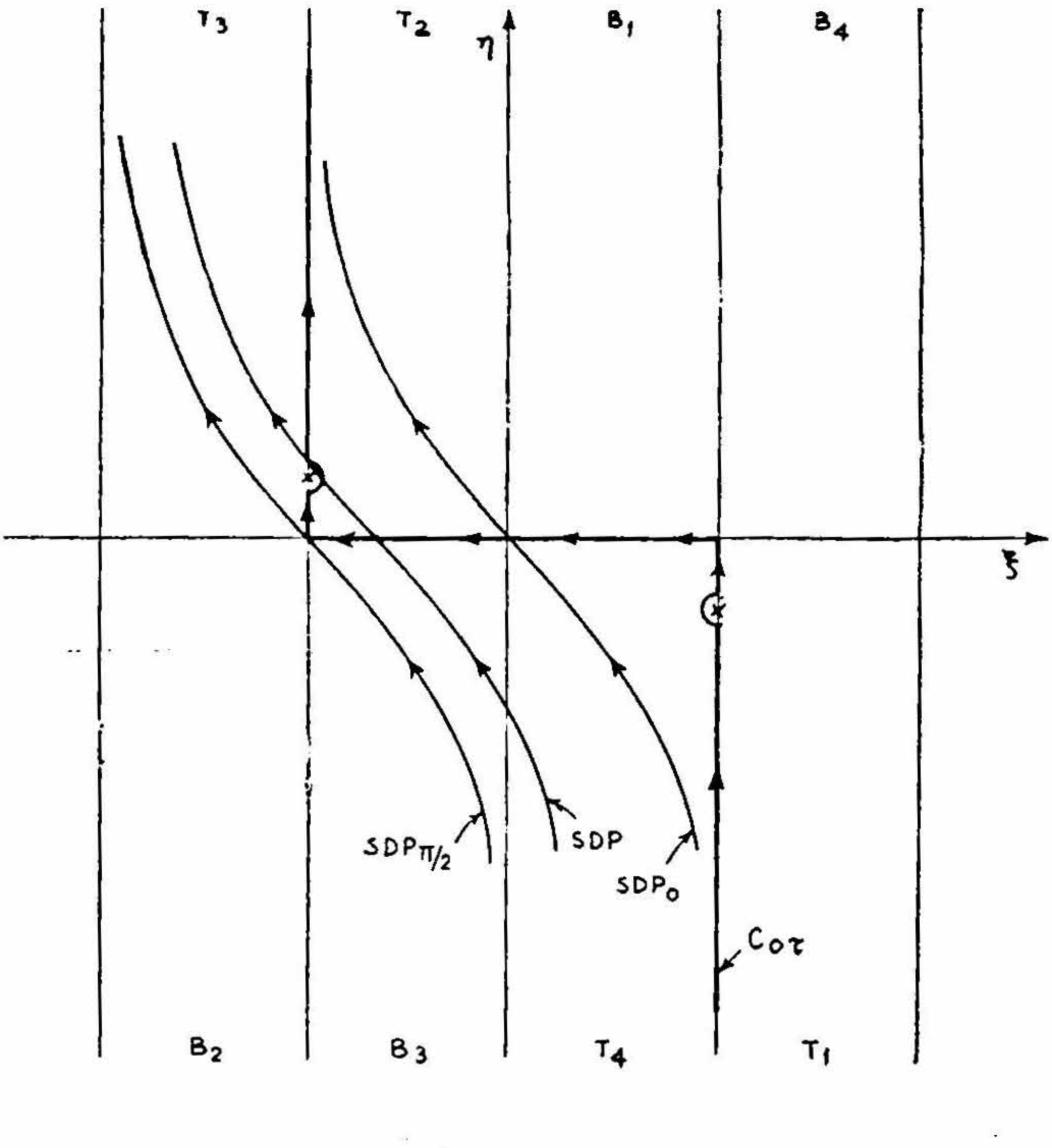


FIG. 18. Steepest descent paths and the map of $C_0$ on the $\tau$-plane for the case of $z$ less than zero.

which is evaluated by using the contour shown in Fig. 17. The transformation $z = r \sin\theta$, $x - (a + d) = r \cos\theta$ has been used, $\theta$ varying from 0 to $-\pi/2$ (Fig. 1). On the $\tau$-plane, $SDP$ varies from $SDP_0$ to $SDP - \pi/2$ (Fig. 18). The original contour from $+\infty$ to $-\infty$ is shown in Fig. 17 and the $SDP$'s are oriented as in Fig. 18. The following poles will be captured.

(*a*) Complex poles on $\xi = -\pi/2$ with greater than zero. These are surface wave poles which are given by roots of $f_1(\omega) = 0$. On the $h$-plane, they are real poles lying between $-k_0$ and $-k$.

(*b*) The complex roots in the strip $B_3$. These give leaky waves.

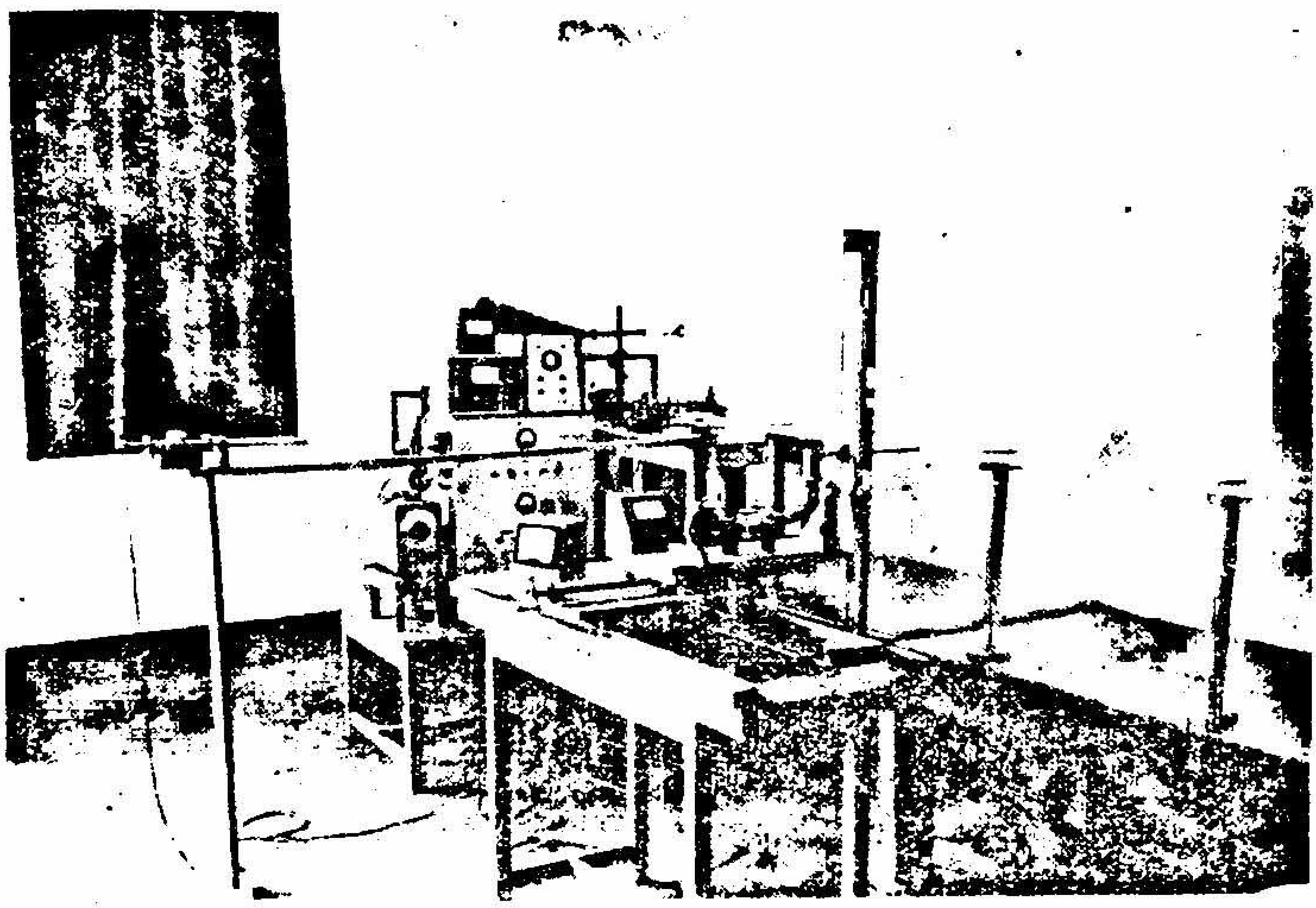

FIG. 19 Photograph of the Experimental set-up.

## 8. LIMITATIONS OF THE THEORY

The accuracy in the evaluation of the field depends on the accuracy with which the poles of the integrand can be determined and also on the limit of accuracy of the Gaussian quadrature method [19] which has been used to calculate the complementary error function involved in the modified saddle-point method. The assumption that the dielectric plates are lossless may also introduce a certain error in determining the roots of the equation $X = 0$.

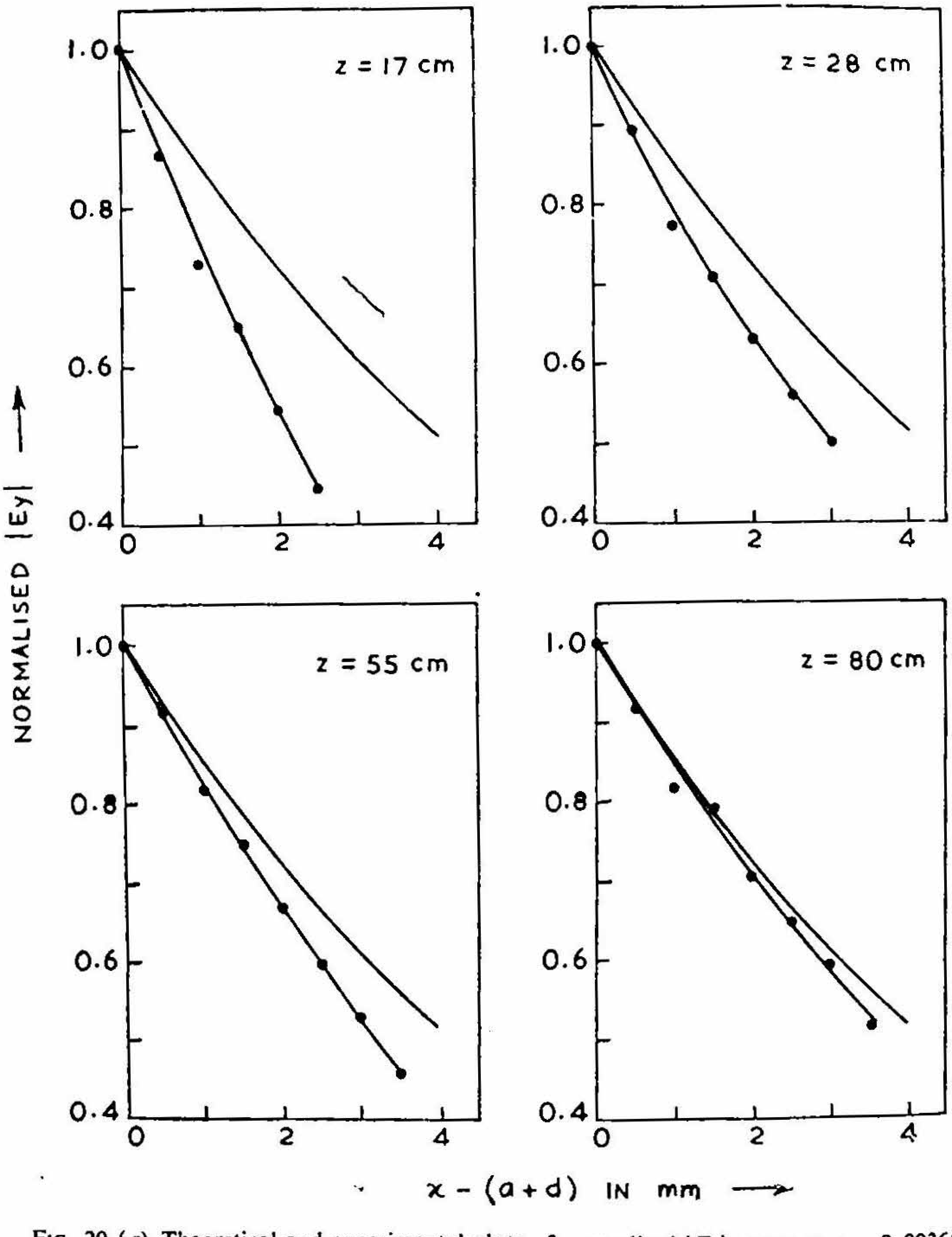


FIG. 20 (*a*). Theoretical and experimental plots of normalised $|E_y|$ versus $x$. $a = 0{\cdot}00365$ m, $d = 0{\cdot}0064$ m, $k_0 = 200$ radians per metre, $k = 320$ radians per metre. $z = 0$: Source or mouth of exciting guide. Values of $z$ indicated in the graph. ——— Theoretical; ●———● Experimental.

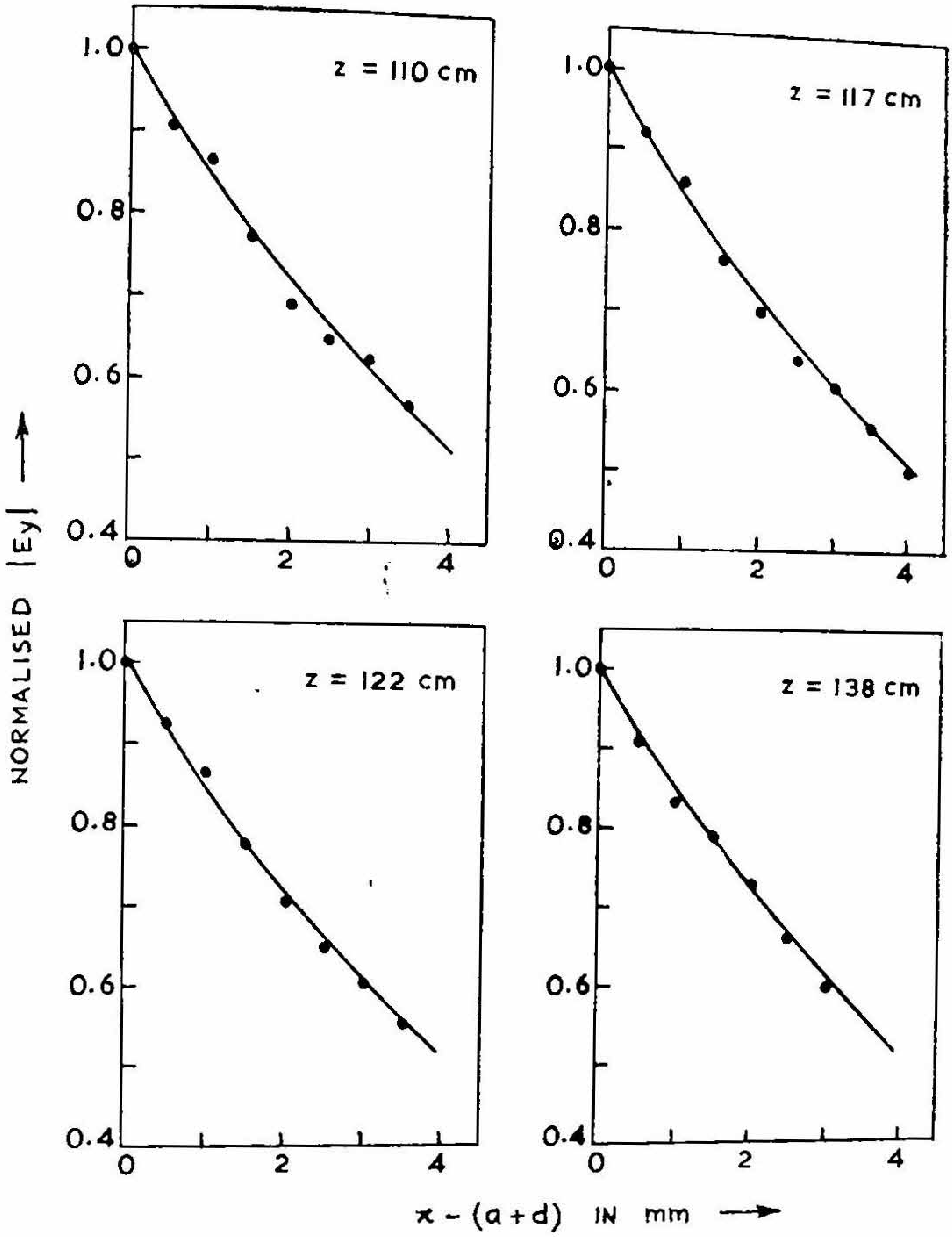


FIG. 20 (*b*). Theoretical and experimental plots of normalised $|E_y|$ versus $x$. $a = 0{\cdot}00365$ metre, $d = 0{\cdot}0064$ m, $k_0 = 200$ radians per metre, $k = 320$ radians per metre. $z = 0$: Source or mouth of exciting guide. Values of $z$ indicated in the graph. ——— Theoretical; * * Experimental points.

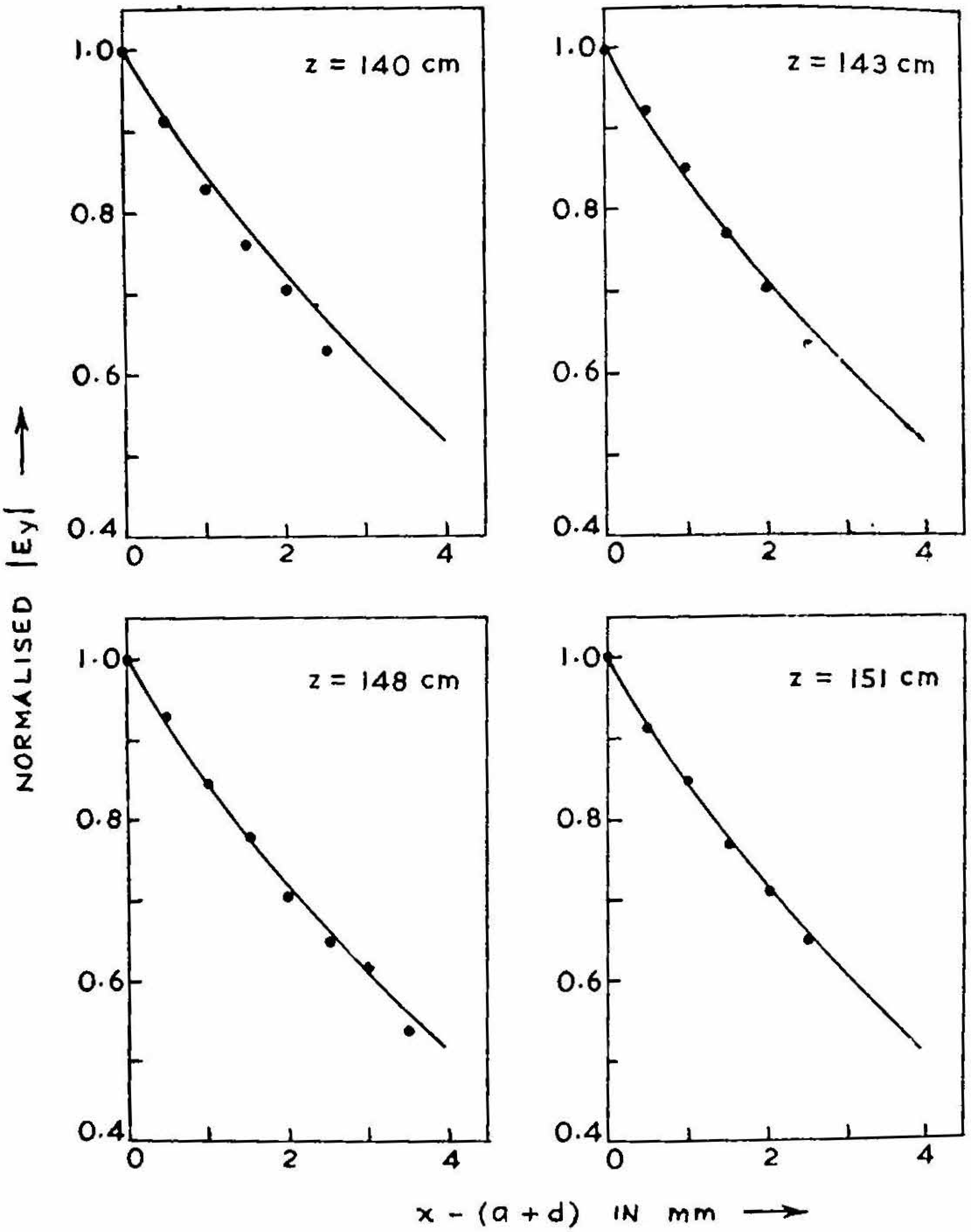


FIG. 20 (c). Theoretical and experimental plots of normalised $|E_y|$ versus $x$. $a = 0{\cdot}00365$ m, $d = 0{\cdot}0064$ m, $k_0 = 200$ radians per metre, $k = 320$ radians per metre. $z = 0$: Source or mouth of exciting guide. Values of $z$ indicated in the graph. —— Theoretical; • • Experimental points.

## 9. Experimental Verification of the Theory

The experimental arrangement for field measurements in the $z$, $x$ and $\theta$ directions by using the usual probe technique is shown in the photograph (Fig. 19).

Figures 20–24 show comparison between theory and experiment.

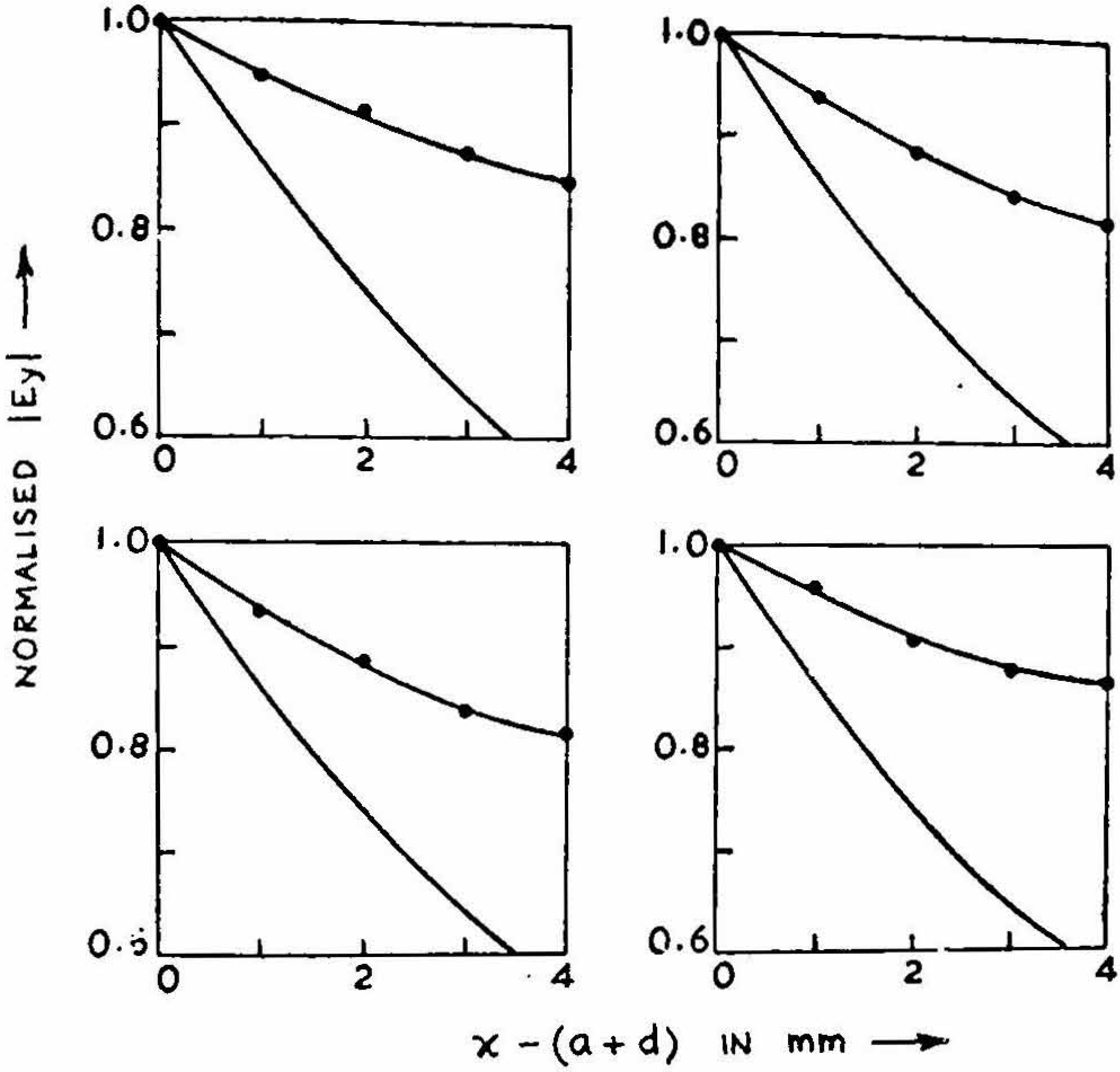


Fig. 21. Theoretical and experimental plots of normalised $|E_y|$ versus $x - (a + d)$ for different values of $z$. $a = 0{\cdot}02$ m, $d = 0{\cdot}0064$ m, $k_0 = 200$ radians per metre, $k = 320$ radians per metre. ——— Theoretical; ●—● Experimental.

## 10. Discussion

(i) The infinite extension of the line source in the theory is simulated in practice by terminating the parallel dielectric plates in the $y$-direction by two metal plates placed in intimate contact with the dielectric plates so as to be normal to the electric field. The parallel dielectric plates extend to

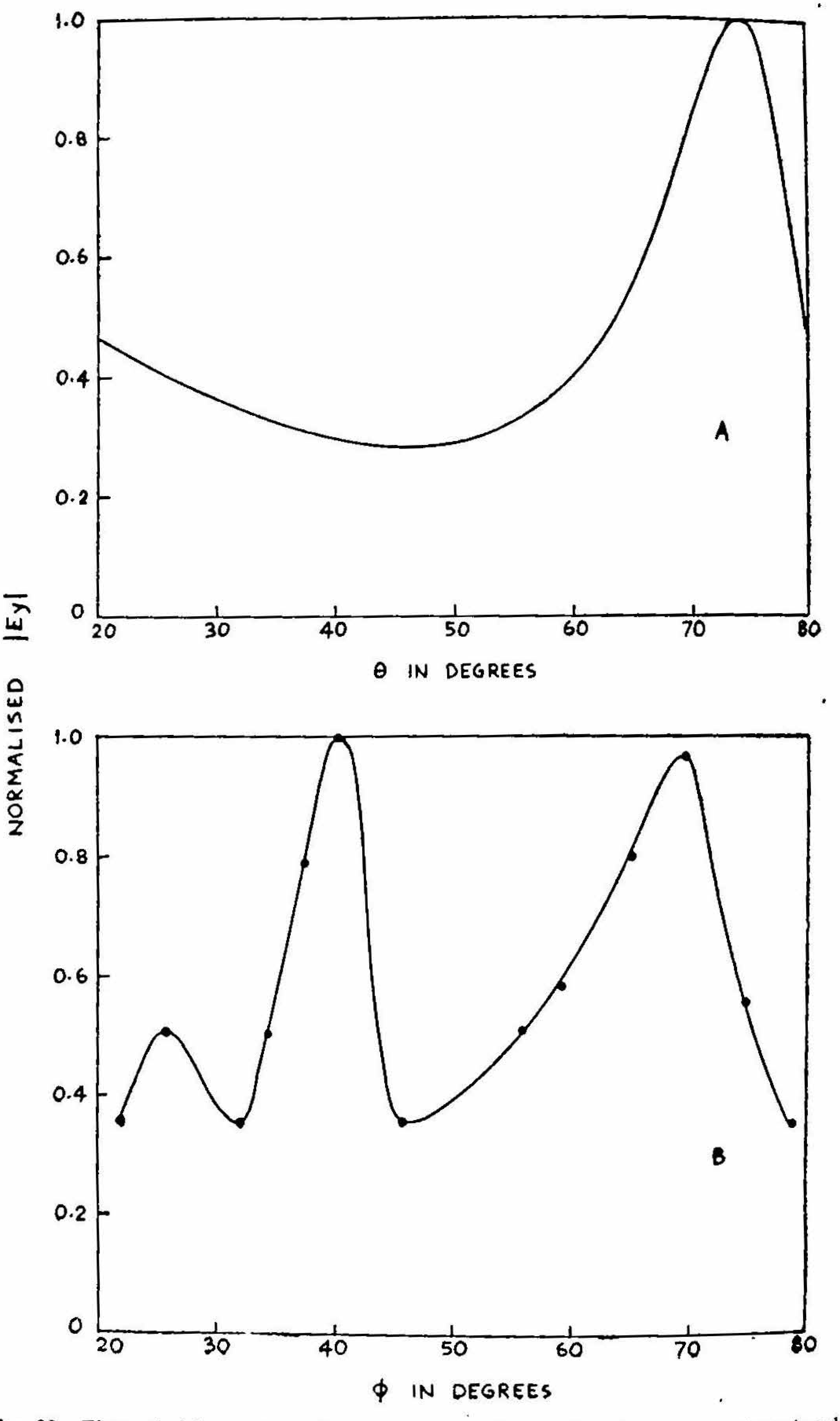


FIG. 22. Theoretical (A) and experimental (B) plots of normalised $| E_y |$ *versus* the azimuthal angle. $r = 1$ metre in both cases, $a = 0 \cdot 02$ m, $d = 0 \cdot 0064$ m, $k_0 = 200$ radians per metre, $k = 320$ radians per metre.

about $80\lambda_0$ in the $z$-direction. The measurement of the field in the $y$-direction shows that $| E_y |$ is practically uniform. So it may be considered that the top and bottom terminating metal plates help to simulate the infinite line source satisfactorily.

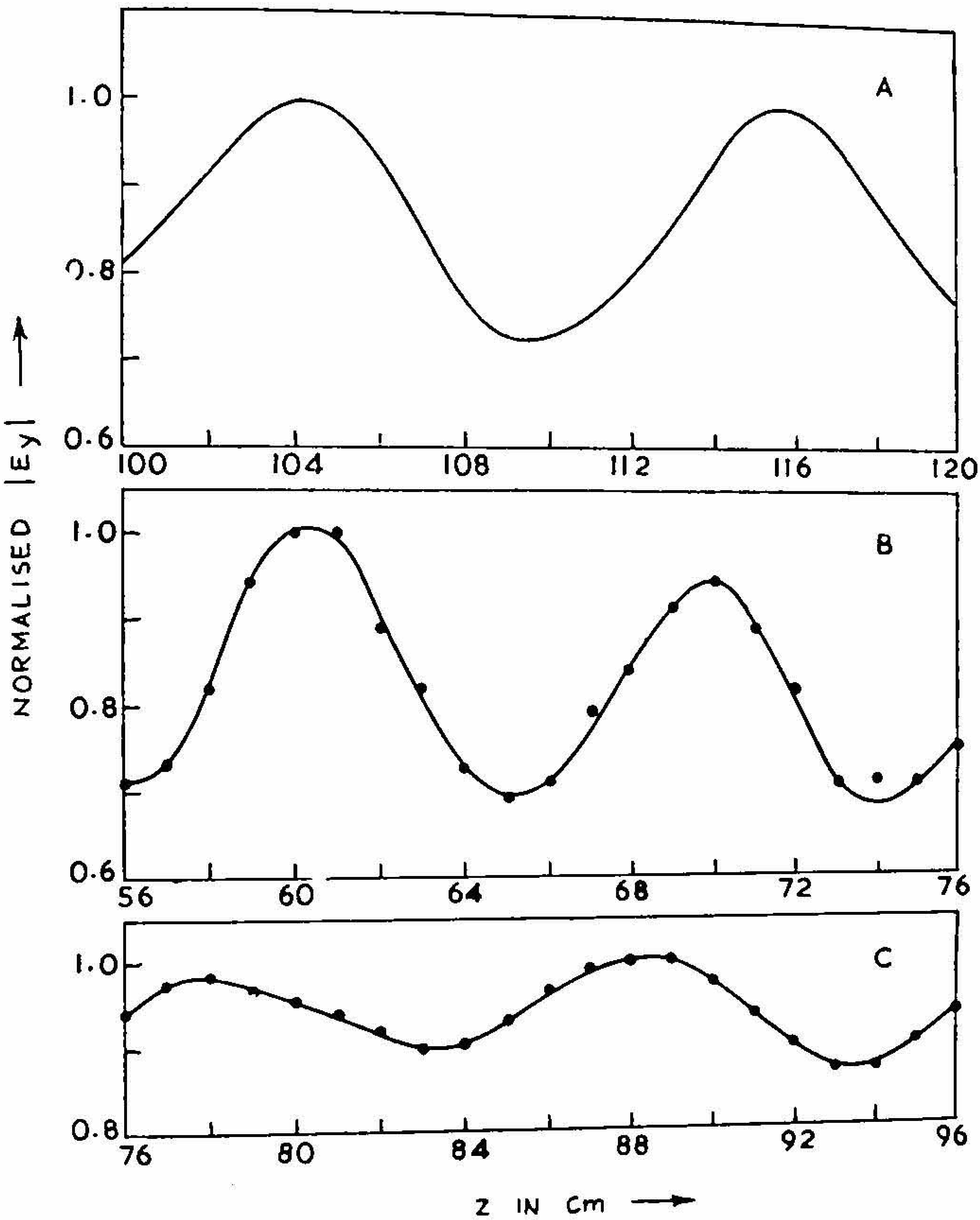


FIG. 23. Theoretical (A) and experimental (B and C) plots of normalised $| E_y |$ versus $z$. $z = 0$: Source in theory, mouth of the exciting metal guide in experiment. $a = 0{\cdot}02$ m, $d = 0{\cdot}0064$ m, $k_0 = 200$ radians per metre, $k = 320$ radians per metre. $x - (a + d) = 2$ mm.

(ii) In the case of the spacing between the plates $a = 0 \cdot 02$ m the distance between any two consecutive minima of the interference pattern is of the order of 10 cm (Fig. 20 *a*) as predicted by theory which is valid for $z > 1$ m. The measurement had to restricted to a distance $z > 1$ m due to the limited sensitivity of the detecting system. In the range $z = 56$–76 cm, the distance between any two consecutive minima is $9 \cdot 5$ cm (Fig. 20 *b*) but in the range $z = 76$–96 cm, it is 10 cm (Fig. 20 *c*).

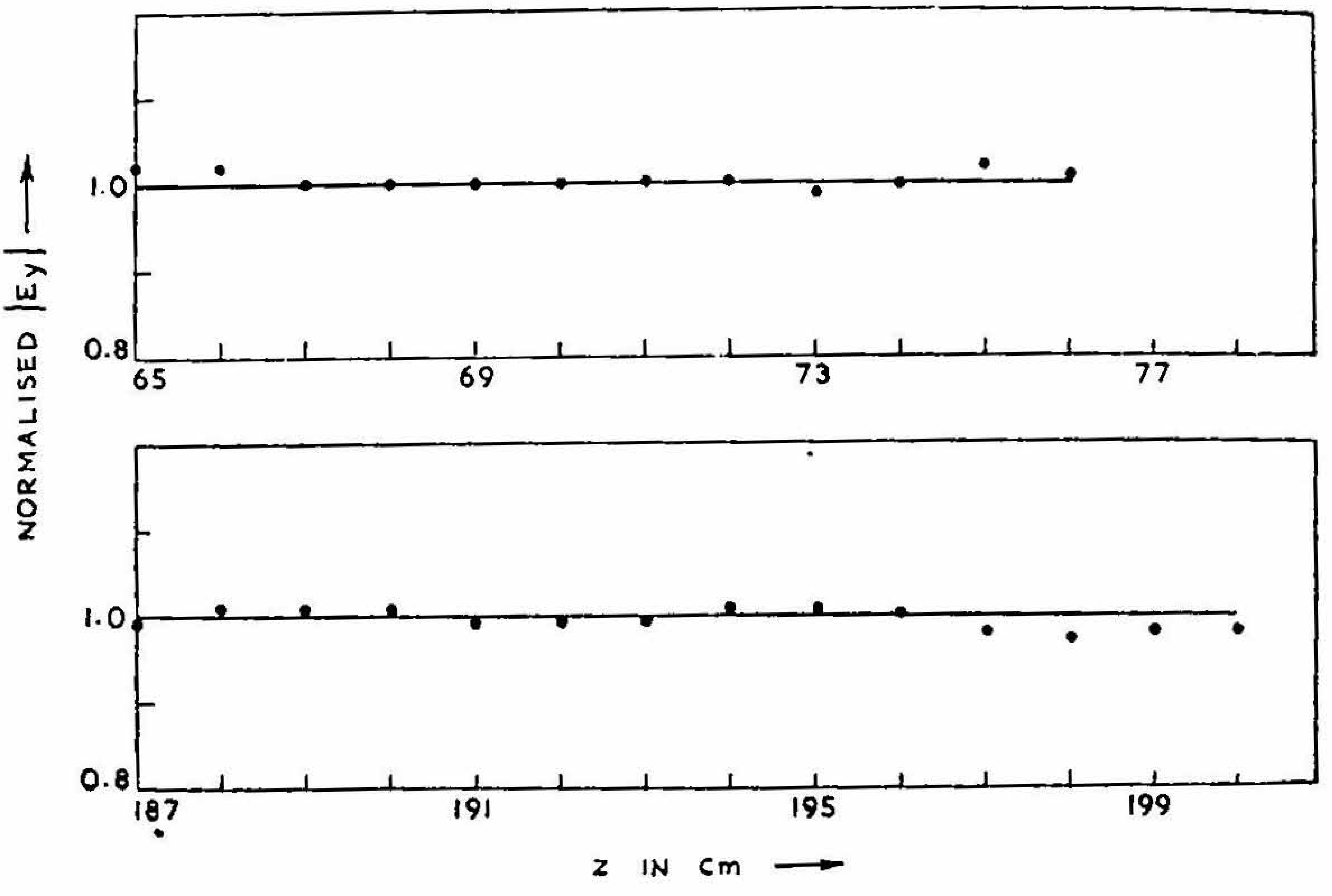


FIG. 24. Theoretical and experimental plots of normalised $|E_y|$ versus $z$. $z = 0$: Source or mouth of exciting metal guide. $a = 0 \cdot 00365$ m, $d = 0 \cdot 0064$ m, $k_0 = 200$ radians per metre, $k = 320$ radians per metre. —— Theoretical; • • Experimental points.

(iii) When $a = 0 \cdot 00365$ m, the theory predicts the existence of only the surface wave mode and non-existence of any significant leaky wave mode. The space wave term also is very small. This is confirmed by experiment which does not show any interference pattern (Fig. 21).

(iv) The variation of the field with respect to $x$ (Fig. 22) shows that agreement with theory becomes closer as $z$ approaches and exceeds 1 m. This is expected as the approximations in the saddle-point method used for evaluating the field numerically improve for larger and larger values of $z$.

(v) For higher spacings, *e.g.*, $a = 0 \cdot 02$ m, the decay characteristics are not that of surface wave (Fig. 23) due to the existence of other modes in addition to the surface wave. The theoretical curves in Fig. 23 show the characteristics of surface wave.

(vi) In the theoretical evaluation of the field in the azimuthal direction the origin of the polar coordinate system is located at the point of intersection of the $x$-axis and outer surface of one of the dielectric plates. In the experimental work, the origin of the polar coordinate system coincides with the pivot of the rotating arm. The position of the pivot is on the axis of the guide. This gives rise to a certain amount of discrepancy in the location of the peaks in the azimuthal direction. The difference between the theoretical angle $\theta$ and the experimental angle is about 1° at a radial distance of 1 m.

The azimuthal plot (Fig. 24) shows that a lobe occurs at 70°. If the origin of the polar coordinate is shifted to the same point assumed in the theoretical discussion, then this lobe would have occurred at 71°. The theoretical value is 74° due to the leaky wave mode. This difference remains to be explained.

The second lobe observed at 40° in the experimental plot is probably due to the radiation from the dielectric wedge which is used for launching the waves in the dielectric guide.

## 11. Conclusions

The propagation characteristics of a parallel-plate dielectric wave guide excited by an electric line source have been investigated. The analysis provides an understanding of the conditions under which the field exhibit the nature of surface wave, leaky wave or radiated wave depending on the spacing between the two parallel plates. It is concluded that

(i) for small spacing such as $a = 0 \cdot 00365$ m only the surface wave is predominant.

(ii) for larger spacing such as $a = 0 \cdot 02$ m leaky wave appears in addition to the surface wave.

It is hoped that the results of the present investigations will add to our existing knowledge of the anatomy of source excited fields on open type of electromagnetic structures.

## 12. ACKNOWLEDGEMENT

The authors wish to thank Dr. S. Dhawan, Director, for providing the necessary facilities for this investigation and to Dr. Unger and Dr. Clarricoat for helpful suggestions.

## 13. REFERENCES

[1] Brown, J. .. *IRE Trans.*, Vol. AP-7, Special Supplement, S 169, 1959.

[2] Whitmer, R. M. .. *Proc. IRE*, 1948, 36, 1105.

[3] Cohn, M. Cassedy, E. S. and Kott, M. A. *IRE Trans.*, 1960, Vol. MTT-8, 545.

[4] Tai, C. T. .. *Journal of Applied Physics*, 1951, 32, 405.

[5] Barone, S. .. *Microwave Res. Rep.*, Polytechnic Institute of Brooklyn, R-532-56, PIB-462, 1956.

[6] Barone, S. and Hessel, A. *Microwave Res. Rep.*, 1958, PIB-626, R-698-58, 1958.

[7] Stickler, D. C. .. *Ohio State University Res. Foundation Rep.*, 1958, 786-2.

[8] Bernard, G. D. and Ishimaru, A. *Proc. IEE*, 1967, 114, 43.

[9] Janes R. Wail .. *J. Res. Natl. Bur. Stds.*, 1957, 59, 365.

[10] Collin, R. V. .. *Field Theory of Guided Waves*, 1960. Published by McGraw-Hill Book Co.

[11] Cullen, A. L. .. *Proc. IEE*, 1954, Vol. 101, Pt. IV, 225.

[12] Karbowiak, A. E. .. *IRE Trans.*, 1959, AP-7, S-191.

[13] Tanir, T. and Oliver, A. A. *Proc. IEE*, 1963, 110, 310, 325.

[14] Rajeswari, B. V. and Chatterjee, S. K. *Journal of Indian Institute of Science*, 1969, 51, 21.

[15] Chatterjee, S. K. .. *Journal of Institute of Engineers (India)*, 1965, 46, 13,

[16] Zucker, F. J. .. *Proc. Symp. Modern Advances in Microwave Technique*, 1954, p. 403.

[17] Vander Weerden, B. L. .. *Appl. Sci. Res.*, 1950, 2B, 33.

[18] Clemmow, P. C. .. *Quart. J. Mech. and Appl. Math.*, 1950, 3, 241.

[19] Erdelyi, A,. Magnus, W. and Obertinger, F, *Tables of Integral Transforms*, Vol. 1, Bateman Project. McGraw-Hill Book Co., 1954.

## APPENDIX A. 1

$$D = \begin{vmatrix} A_{11} & A_{12} & \cdots\cdots & A_{19} & A_{110} \\ A_{21} & A_{22} & \cdots\cdots & A_{29} & A_{210} \\ \cdots & \cdots & & & \\ \cdots & \cdots & & & \\ \cdots & \cdots & & & \\ \cdots & \cdots & & & \\ \cdots & \cdots & & & \\ \cdots & \cdots & & & \\ A_{91} & A_{92} & \cdots\cdots & A_{99} & A_{910} \\ A_{101} & A_{102} & \cdots\cdots & A_{109} & A_{1010} \end{vmatrix}$$

$Dr$ is the det. $D$ with the $r$-th column replaced by the column

$$\begin{vmatrix} 0 \\ 0 \\ 0 \\ 0 \\ 0 \\ -\tfrac{1}{2}\pi \\ 0 \\ 0 \\ 0 \\ 0 \end{vmatrix}$$

where

$$A_{11} = \exp\{-p(a+d)\}, \qquad A_{21} = p\exp\{-p(a+d)\}$$

$$A_{31} = A_{41} = \ldots = A_{10,\,1} = 0$$

$$A_{12} = -\exp\{-q(a+d)\}, \qquad A_{22} = -q\exp\{-q(a+d)\}$$

$$A_{32} = \exp(-qa), \qquad A_{42} = q\exp(-qa)$$

$$A_{52} = A_{62} = \ldots = A_{10,\,2} = 0$$

$$A_{13} = -\exp\{q(a+d)\} \qquad A_{23} = q\exp\{q(a+d_{23})\}$$

$$A_{33} = \exp(qa) \qquad A_{43} = -q\exp(qa)$$

$$A_{53} = A_{63} = \ldots = A_{10,3} = 0$$

$$A_{14} = A_{24} = 0, \quad A_{34} = -\exp(-pa), \quad A_{44} = -p\exp(-pa)$$

$$A_{54} = 1, \quad A_{64} = -p, \quad A_{74} = \ldots = A_{10,4} = 0$$

$$A_{15} = A_{25} = 0, \quad A_{35} = -\exp(pa), \quad A_{45} = p\exp(pa)$$

$$A_{55} = 1, \quad A_{65} = p, \quad A_{75} = \ldots = A_{10,5} = 0$$

$$A_{16} = \ldots = A_{46} = 0, \quad A_{56} = -1, \quad A_{66} = p$$

$$A_{76} = \exp(pa), \quad A_{86} = p\exp(pa), \quad A_{9,6} = A_{10,6} = 0$$

$$A_{17} = \ldots = A_{47} = 0, \quad A_{57} = -1, \quad A_{67} = -p$$

$$A_{77} = \exp(-pa), \quad A_{87} = -p\exp(-pa), \quad A_{97} = A_{10,7} = 0$$

$$A_{18} = \ldots = A_{68} = 0, \quad A_{7,8} = \exp(qa), \quad A_{88} = -q\exp(qa)$$

$$A_{98} = \exp\{q(a+d)\}, \quad A_{10,8} = q\exp\{q(a+d)\}$$

$$A_{19} = \ldots A_{69} = 0, \quad A_{79} = -\exp(-qa), \quad A_{89} = q\exp(-qa)$$

$$A_{99} = \exp\{-q(a+d)\}, \quad A_{10,9} = -q\exp\{-q(a+d)\}$$

$$A_{1,10} = \ldots = A_{8,10} = 0, \quad A_{9,10} = -\exp\{-p(a+d)\}$$

$$A_{10,10} = p\exp\{-p(a+d)\}.$$

## A. 2. SUCCESSIVE BISECTION METHOD

If $x_1$ and $x_2$ represent two values of $x$ such that they are on either side of a root $x_0$ of $f(x)$, then, if $f(x_1)$ is positive, $f(x_2)$ will be negative or *vice versa*. The value of $f(x)$ is determined at $x_3 = (x_1 + x_2)/2$. If there is a change of sign in $f(x)$ between $x_1$ and $x_3$, then $x_0$ lies between $x_1$ and $x_3$. If $f(x)$ changes sign between $x_2$ and $x_3$, then the root lies in the interval $(x_3, x_2)$. The function is evaluated again at $x_4 = (x_3 + x_i)/2$ where, $i = 1$ or 2. according as the root lies between $x_1$ and $x_3$ or $x_2$ and $x_3$. This iterative procedure is repeated until the value of $f(x)$ is smaller than a prescribed small number. Then the value of $x$ at which $f(x)$ is small will be equal to the root. The smaller the value of $f(x)$ the greater the accuracy of the root that is obtained.

## A. 3. EVALUATION OF $E_y$

In equations (44)–(46)

$$F(\theta) = q(\theta)\,\frac{k_0 \cos\theta}{\pi x(\theta)}$$

$$q = (k_0^2 \sin^2 \theta - k^2)^{\frac{1}{2}}$$

$$b^2 = k^2 - k_0^2$$

$$erfc = 1 + \frac{iz}{\sqrt{\pi}} \{u(\rho, \theta) + iv(\rho, \theta)\}$$

$$iz = \rho \exp(i\theta)$$

$$u(\rho, \theta) = \int_0^\rho \exp(t^2 \cos 2\theta) \cos(t^2 \sin 2\theta + \theta)\, dt$$

$$v(\rho, \theta) = \int_0^\rho \exp(t^2 \cos 2\theta) \sin(t^2 \sin 2\theta + \theta)\, dt$$

All the constant $k_0$, $a$, $d$, $k$, $\epsilon_i$ except $A_{0i}'$ and $\tau_{0i}'$ are real. A residue $R_j = A_{0j} \exp\{ik_0 r \cos(\tau_{0j} - \theta)$ is added to $E_y$ when $\theta > \theta_{0j}$. When $\theta = \theta_{0j}$ $R_j/2$ is added to $E_y$.